Feinstein College of Arts & Sciences Faculty
Publications

Feinstein College of Arts and Sciences

2012

A deep search for the host galaxies of gamma-ray bursts with no detected optical afterglow

A. Rossi

S. Klose

P. Ferrero

J. Greiner

L.A. Arnold

See next page for additional authors

Follow this and additional works at: http://docs.rwu.edu/fcas_fp

Part of the Astrophysics and Astronomy Commons

Recommended Citation

Authors

A. Rossi, S. Klose, P. Ferrero, J. Greiner, L.A. Arnold, E. Gonsalves, D.H. Hartmann, Adria Updike, D.A. Kann, T. Krühler, E. Palazzi, S. Savaglio, S. Schulze, P.M.J. Afonso, L. Amati, A.J. Castro-Tirado, C. Clemens, R. Filgas, J. Gorosabel, L.K. Hunt, A. Küpcü Yoldas, N. Masetti, M. Nardini, A. Nicuesa Guelbenzu, F.E. Olivares, E. Pian, A. Rau, P. Schady, S. Schmidl, A. Yoldas, and A. de Ugarte Postigo

Astronomy & Astrophysics

A deep search for the host galaxies of gamma-ray bursts with no detected optical afterglow[⋆,⋆⋆]

A. Rossi[1], S. Klose[1], P. Ferrero[2,3], J. Greiner[4], L. A. Arnold[5], E. Gonsalves[6], D. H. Hartmann[7], A. C. Updike[8], D. A. Kann[1], T. Krühler[4,9,10], E. Palazzi[11], S. Savaglio[4], S. Schulze[12], P. M. J. Afonso[13], L. Amati[11], A. J. Castro-Tirado[14], C. Clemens[4], R. Filgas[4,15], J. Gorosabel[14], L. K. Hunt[16], A. Küpcü Yoldaş[17], N. Masetti[11], M. Nardini[18], A. Nicuesa Guelbenzu[1], F. E. Olivares[4], E. Pian[11,19,20], A. Rau[4], P. Schady[4], S. Schmidl[1], A. Yoldaş[17], and A. de Ugarte Postigo[10,14]

(Affiliations can be found after the references)

ABSTRACT

Context. Gamma-ray bursts (GRBs) can provide information about star formation at high redshifts. Even in the absence of a bright optical/near-infrared/radio afterglow, the high detection rate of X-ray afterglows by *Swift*/XRT and its localization precision of 2–3 arcsec facilitates the identification and the study of GRB host galaxies.

Aims. We focus on the search for the host galaxies of 17 bursts with arcsec-sized XRT error circles but no detected long-wavelength afterglow, in spite of their deep and rapid follow-up observations. Three of these events can also be classified as truly dark bursts, i.e., the observed upper limit on the optical flux of the afterglow was less than expected based on the measured X-ray flux. Our goals are to identify the GRB host galaxy candidates and characterize their phenomenological parameters.

Methods. Our study is based on deep R_C and K_s-band observations performed with FORS1, FORS2, VIMOS, ISAAC, and HAWK-I at the ESO/VLT, partly supported by observations with the seven-channel imager GROND at the 2.2-m telescope on La Silla, and supplemented by observations with NEWFIRM at the 4-m telescope on Kitt Peak. To be conservative, we searched for host galaxy candidates within an area of twice the radius of each associated 90% c.l. *Swift*/XRT error circle.

Results. For 15 of the 17 bursts, we find at least one galaxy within the searching area, and in the remaining two cases only a deep upper limit to R_C and K_s can be provided. In seven cases, we discover extremely red objects in the error circles, at least four of which might be dust-enshrouded galaxies. The most remarkable case is the host of GRB 080207, which has a color of $(R_C − K_s)_{AB} \sim 4.7$ mag, and is one of the reddest galaxies ever associated with a GRB. As a by-product of our study we identify the optical afterglow of GRB 070517.

Conclusions. Only a minority of optically dim afterglows are due to Lyman dropout ($\lesssim 1/3$). Extinction by dust in the host galaxies might explain all other events. Thereby, a seemingly non-negligible fraction of these hosts are globally dust-enshrouded, extremely red galaxies. This suggests that at least a fraction of GRB afterglows trace a subpopulation of massive starburst galaxies, which are markedly different from the main body of the GRB host galaxy population, namely the blue, subluminous, compact galaxies.

Key words. gamma-ray burst: general – galaxies: high-redshift

1. Introduction

1.1. Optical afterglows

By the end of 2010, about 900 gamma-ray bursts (GRBs) have been localized at the arcmin scale (see Greiner's www page[1]), most of them (>80%) by the *Swift* satellite (Gehrels et al. 2004). Nearly 600 events have a detected X-ray afterglow, and nearly 400 have been detected in the optical and near-infrared (NIR) bands, too. The observed brightness distribution of the optical afterglows is broad and time-dependent, spanning at least

14 mag within the first hour after the burst, and at least 10 mag at around 1 day, after correction for Galactic extinction (Kann et al. 2010, 2011).

In principle, the observed brightness distribution reflects the luminosity distribution of the afterglows (an intrinsic property), but it is affected by physical processes that can block the optical light on its way to the observer (external processes). The latter consists of two possible mechanisms, extinction by dust in the GRB host galaxies (GRBHs) represented by the parameter A_V^{host}, and cosmological Lyman absorption owing to the high redshift of the objects. If an afterglow is still detected in the optical/NIR bands, these two processes can be recognized if a redshift (z) can be measured and a broad-band spectral energy distribution (SED) of an afterglow constructed. The analysis of optically detected afterglows shows that (in the *R* band) Lyman absorption is rather the exception than the rule; only a small fraction of bursts lie at $z \gtrsim 5$ (cf. Haislip et al. 2006; Kawai et al. 2006; Tagliaferri et al. 2005; Greiner et al. 2009; Tanvir et al. 2009; Salvaterra et al. 2009; Pérez-Ramírez et al. 2010; Cucchiara et al. 2011). In addition, it is found that while extinction by dust in GRBHs along the lines of sight is usually rather small, a long tail of

possible extinction values is apparent in the data (cf. Kann et al. 2010; Greiner et al. 2011; Krühler et al. 2011), implying that at least some optical afterglows are extinguished by dust in their host galaxies.

Even if no spectrum of the afterglow can be obtained, a precise optical localization usually means that a search for an underlying host galaxy can be undertaken and, if successful, its redshift can be measured even years after the corresponding burst. The host extinction along the line of sight can then be measured if a broad-band SED of the afterglow can be constructed. In principle, the influence of Lyman dropout and host extinction on the observed SED can be then distinguished from each other (e.g., Rossi et al. 2008a, 2011). However, the precise interplay between intrinsic luminosity, redshift, and host extinction cannot be determined in an easy way if no optical/NIR afterglow is detected at all.

1.2. Bursts with optically undetected afterglows

The reason why a non-negligible fraction of bursts have no optically detected afterglow despite a rapid localization in X-rays on the arcsec scale has been unclear for many years. While many of these non-detections are simply due to the lack of rapid and deep optical follow-up observations, some events (after correction for Galactic extinction) are truly optically dark (e.g., Fynbo et al. 2001; De Pasquale et al. 2003; Castro-Tirado et al. 2007; Rol et al. 2007; Hashimoto et al. 2010; Holland et al. 2010).

Theoretically, the shape of the SED of an afterglow is well-defined and the flux expected in the optical bands is determined by the observed X-ray flux. A comparison with observed optical upper limits can then tell us whether the observations did not go deep enough or if an additional dimming of the afterglow light is required (Rol et al. 2005; Jakobsson et al. 2004; van der Horst et al. 2009). Once the real dark nature of a GRB is established, the question is which of the aforementioned three physical mechanisms led to the non-detection in the optical bands. To tackle this problem, one can try to identify the most likely GRB host candidate within the corresponding X-ray error circle and study the corresponding galaxy population.

After a putative host has been identified, the observations can constrain not only the redshift but may also help to explain the optical dimness of the afterglow Several studies of individual events have already found that dust extinction in the corresponding GRBHs was the main reason for the optical dimness of some events (e.g., Piro et al. 2002; Gorosabel et al. 2003; Levan et al. 2006; Berger et al. 2007; Küpcü Yoldaş et al. 2010; Krühler et al. 2011). This conclusion then naturally leads to the question of whether extinction by cosmic dust can explain the entire ensemble of optically dark bursts or whether their high redshifts (seen as Lyman dropouts) is also an important factor. This question was finally answered when Greiner et al. (2011), based on a homogeneous data set of multi-color follow-up observations of bursts, were able to show that extinction by dust in the GRBHs is the main reason for the optical dimness of most dark events. This was later confirmed by Melandri et al. (2012) in an independent analysis of a complete sample of bright *Swift* bursts.

1.3. The present work

Even though the dominant role of extinction in explaining optically dim/dark events has long been established, we still wish to identify and characterize the host galaxies of all bursts with no detected long-wavelength afterglow at all. Therefore, in the

case of *Swift* bursts, host galaxies have to be identified in X-ray error circles with sizes on the order of some arcsec, which is still observationally challenging and usually requires the largest optical telescopes. A first study of this kind was published by Perley et al. (2009), who reported on the results of an imaging campaign at Keck Observatory. In their analysis, they focused on a homogeneous sample of 29 *Swift* GRBs with rapid follow-up observations by the robotic Palomar 60 inch telescope (Cenko et al. 2009), among which seven were undetected by the P60 down to $R = 20-23$ only 1 ks after the burst. They found that a significant fraction of the afterglows in their sample was affected by host extinction at moderate redshift and were able to constrain the fraction of high-z *Swift* events to at most 7% (at the 80% c.l.[2]). In particular, on the basis of mainly optical observations they concluded that the hosts of dark bursts seem to be rather normal galaxies in terms of their colors, suggesting that the obscuring dust is rather local to the vicinity of the GRB progenitor or highly unevenly distributed within the host galaxy.

Here, we report on the results of a search for the potential hosts of 17 bursts with no detected optical/NIR afterglow. All bursts in our sample have an observed duration in the *Swift*/BAT (Barthelmy et al. 2005) energy window of $T_{90} > 2$ s, i.e., they are classified as long GRBs (Kouveliotou et al. 1993). All events have optical upper limits well below the average brightness of detected long-GRB afterglows (Kann et al. 2010). Our goal is to identify the host-galaxy candidates and to study the galaxy population of these events in order to ascertain more clearly the cause of the optical dimness of the corresponding afterglows. In contrast to Perley et al. (2009), we also make use of deep NIR observations in order to identify and characterize the GRB host galaxy population.

This paper is organized as follows. In Sect. 2, we describe the sample selection and the data-reduction procedures. In Sect. 3, we provide a detailed overview of the objects found in the corresponding *Swift*/XRT (Gehrels et al. 2004; Burrows et al. 2005) error circles. Section 4 then compiles information about these objects and characterizes host-galaxy candidates and subsamples based on different selection criteria. Finally, a summary is given in Sect. 5.

Throughout this work, we adopt the convention that the flux density of the afterglow can be described as $F_\nu(t) \propto t^{-\alpha}\nu^{-\beta}$ and we use a ΛCDM world model with $\Omega_M = 0.27$, $\Omega_\Lambda = 0.73$, and $H_0 = 71$ km s^{-1} Mpc^{-1} (Spergel et al. 2003).

2. Target selection and observations

2.1. The GRB sample

In the years from 2005 to 2008, there were about 100 bursts at a declination ≤ 25 deg (i.e., fields easily observable from either ESO Paranal or La Silla) with detected X-ray afterglows but no detected optical afterglows[3]. From this sample, we selected 17 fields with the following properties: (1) the X-ray error circle radius is smaller than six arcsec, (2) rapid (within one day), deep, but unsuccessful follow-up observations performed by various optical telescopes, and (3) Galactic visual extinction along the line of sight of less than 1 mag. In addition, when we selected these targets (usually several months before they were observed) no corresponding studies had been reported in the literature[4].

---

[2] c.l. stands for confidence level.

[3] See footnote 1.

[4] We have been unable to investigate several other bursts that also fulfil our selection criteria, owing to the limited amount of granted telescope time.

Table 1. Characterizations of the GRB fields of our sample.

#	GRB	T_{90} s	RA, Dec (J2000) XRT	Error arcsec	Galactic coordinates (l, b) degrees	$E(B - V)$ mag
1	050717	85	14:17:24.48, −50:32:00.7	1.5	316.61, 10.04	0.24
2	050922B	150.9	00:23:13.37, −05:36:16.7	1.7	104.35, −67.45	0.04
3	060211A	126.3	03:53:32.65, +21:29:19.0	1.4	169.74, −24.40	0.19
4	060805A	5.3	14:43:43.47, +12:35:11.2	1.6	9.53, 59.97	0.02
5	060919	9.1	18:27:41.80, −51:00:52.1	1.7	343.87, −17.50	0.07
6	060923B	8.6	15:52:46.70, −30:54:13.7	1.8	342.74, 17.61	0.15
7	061102	45.6	09:53:37.84, −17:01:26.0	2.9	253.43, 28.29	0.04
8	070429A	163.3	19:50:48.92, −32:24:17.8	2.1	8.06, −25.90	0.17
9	070517	7.6	18:30:28.93, −62:17:51.7	2.1	332.76,−21.47	0.15
10	080207	340	13:50:02.93, +07:30:07.9	1.4	340.92, 65.95	0.02
11	080218B	6.2	11:51:49.65, −53:05:48.5	1.6	293.94, 8.73	0.17
12	080602	74	01:16:42.17, −09:13:55.9	1.7	142.56, −71.13	0.03
13	080727A	4.9	13:53:33.81, −18:32:40.5	1.6	322.88, 41.91	0.07
14	080915A	14	01:11:47.63, −76:01:13.1	3.7	301.30, −41.04	0.05
15	081012	29	02:00:48.17, −17:38:17.2	1.8	185.87, −71.40	0.02
16	081105	∼10	00:15:48.50, +03:28:15.5	4.8	105.87, −58.22	0.03
17	081204	∼20	23:19:09.13, −60:13:31.7	5.3	321.96, −53.36	0.03

Notes. (1) The *Swift*/XRT positions for GRB 061102 and 070517 are from N. Butlers's webpage (http://astro.berkeley.edu/~nat/swift/xrt_pos.html) (Butler 2007). The XRT position for GRB 080915A, 081105, and 081204 are from Oates et al. (2008b), Beardmore & Cummings (2008), and Mangano et al. (2008a), respectively. All other XRT data are from http://www.swift.ac.uk/xrt_positions/index.php (Evans 2011a,b). (2) The burst duration, T_{90}, was mostly taken from http://heasarc.gsfc.nasa.gov/docs/swift/archive/grbtable/. For GRB 081105, the reference is Cummings et al. (2008), for GRB 080727A it is McLean et al. (2008), and for GRB 081204 it is Götz et al. (2008). (3) The Galactic reddening along the line of sight, $E(B - V)$, was obtained from the NASA Extragalactic Database Coordinate Transformation and Extinction calculator at http://nedwww.ipac.caltech.edu/forms/calculator.html.

All 17 bursts have upper limits to their optical afterglow magnitudes that lie at least 1.5 mag below the mean value of the afterglow brightness distribution (Fig. 1). The observed GRB fields are summarized in Table 1 and further details of the corresponding world-wide observing campaigns are given in Appendix A.

Deep follow-up observations of 14 of these 17 X-ray error circles were performed with VLT/FORS1, FORS2, VIMOS, ISAAC, and HAWK-I[5] in the years 2008 to 2010, months to years after the corresponding burst (Table A.4). Limiting 3σ AB magnitudes were typically $R_C = 26.5$ and $K_s = 23.5$. In the case of GRBs 050717, 060211A, and 060805A, multi-band imaging was performed using GROND on La Silla (Greiner et al. 2008) and, in the case of GRBs 050922B and 060211A, data were obtained using the near-infrared imager NEWFIRM mounted at the 4-m Mayall telescope at Kitt Peak National Observatory (Autry et al. 2003). In the case of GRB 081204, a late *J*-band observation was executed using NTT/SOFI on La Silla (Moorwood et al. 1998b).

2.2. Optical/NIR data analysis

VLT, GROND, and NEWFIRM data were reduced using IRAF tasks[6] and analyzed by performing point-spread function (PSF) and aperture photometry using DAOPHOT and APPHOT (Tody 1993). The procedure is mainly based on the pipeline written to reduce GROND data (Yoldaş et al. 2008; Krühler et al. 2008). Aperture photometry, if not otherwise specified, was performed by using an aperture diameter of twice the full width half

maximum (FWHM) of the stellar PSF. The ISAAC, HAWK-I, and GROND NIR fields were calibrated using 2MASS field stars. The VLT optical data were calibrated using standard star fields limited to the Vega photometric system, while the calibration performed for the optical $g'r'i'z'$ images of GROND employed SDSS stars (Table A.4).

We used the following transformations between AB and Vega magnitudes: (1) for FORS1, FORS2, and VIMOS, $R_{AB} = R_{Vega} + 0.23$ mag (Klose et al. 2004) and (2) for ISAAC, HAWK-I, and NEWFIRM $K_{AB} = K_{s,Vega} + 1.86$ mag (Klose et al. 2004). For GROND, the Vega-to-AB conversion is $J_{AB} = J_{Vega} + 0.93$ mag, $H_{AB} = H_{Vega} + 1.39$ mag, as well as $K_{AB} = K_{s,Vega} + 1.80$ mag, except for observations after an intervention on the instrument on March 2008, for which $K_{AB} = K_{s,Vega} + 1.86$ mag.

2.3. Adding X-ray data: which bursts are truly optically dark?

According to Jakobsson et al. (2004, hereafter J04), a GRB with a detected X-ray afterglow is considered dark if the spectral slope between the optical and the X-ray regimes obey the relation $\beta_{OX} < 0.5$, while according to van der Horst et al. (2009, hereafter V09) a burst is optically dark if $\beta_{OX} < \beta_X - 0.5$ (see also Rol et al. 2005). Both definitions are suited to identify additional dimming of the optical flux relative to the observed X-ray flux, assuming standard afterglow theory (e.g., Sari et al. 1998).

To determine β_X and β_{OX}, we used the data from the *Swift*/XRT GRB light curve and spectrum repository (Evans et al. 2007, 2009). Optical upper limits and X-ray data were typically not obtained at the same time. We therefore fit the X-ray light curves in order to interpolate the X-ray flux that was contemporaneous with the corresponding optical/NIR upper limits. Thereby, no calibration issues occurred for the optical upper limits for the afterglows of GRBs 070429A, 070517, 080207,
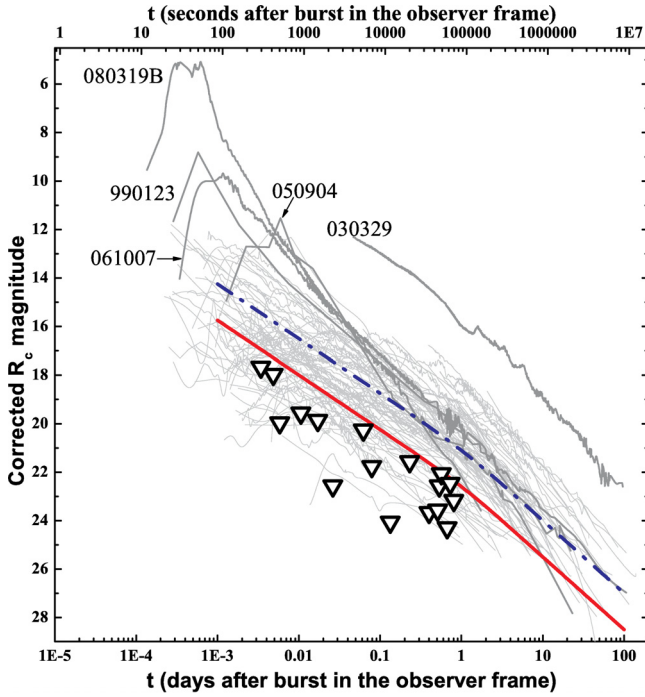
---

[5] See Appenzeller et al. (1998), Le Fèvre et al. (2003), Moorwood et al. (1998a) and Kissler-Patig et al. (2008) for more informations about FORS, VIMOS, ISAAC, and HAWK-I, respectively.
[6] http://iraf.noao.edu

Fig. 1. R_C-band light curves of all (long) afterglows in the sample of Kann et al. (2010, 2011); some extraordinary bright events are indicated. All data have been corrected for Galactic extinction. Triangles indicate equivalent R_C-band upper limits of the afterglows in our sample (Table 2). The blue dashed/dotted line approximately indicates the mean of the afterglow brightness distribution. The red straight line, 1.5 mag below the blue line, indicates the border line of all targets in our study. A colour version of the figure is available in the electronic version.
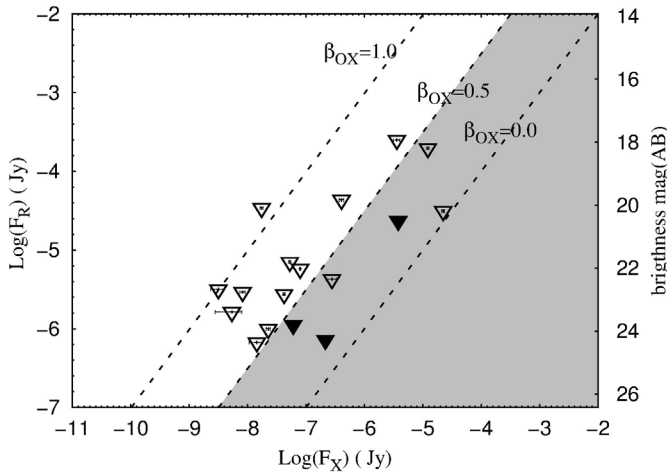

Fig. 2. Application of the J04 criterion: observed upper limits in the R_C band relative to the measured flux density at 1.73 keV (the logarithmic mean of the *Swift*/XRT window, 0.3–10 keV) for the 17 bursts in our sample. When no R_C-band data were available, we used the observed spectral slope β_{OX} to shift the flux density from the native filter to the R band (Table 2). The bursts falling in the gray area fulfil the J04 criterion. The three bursts that can be assumed to be securely classified dark bursts according to J04 as well as V09 (see Fig. 3) are marked with a filled black triangle (see Sect. 2.3).

080218B, 080727A, 080915A, 081012, 081105, and 081204, since here the calibration was performed based on our data sets. In the other cases, optical upper limits were taken from GCN circulars and, therefore, can be affected by systematic errors (e.g., Rossi et al. 2011). Assuming a conservative systematic
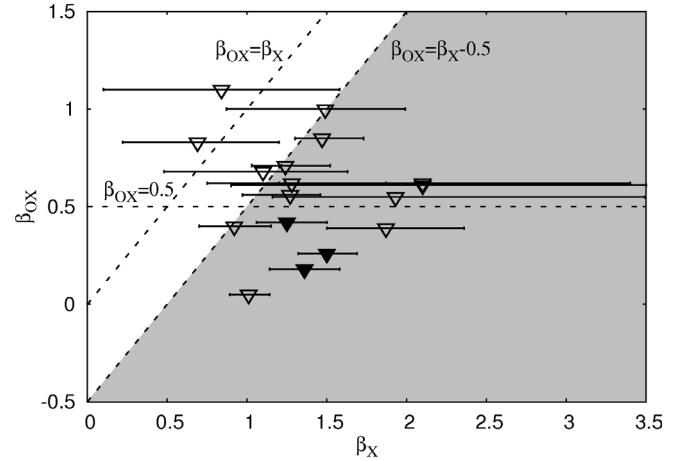
Fig. 3. Application of the V09 criterion: deduced upper limits to the spectral slope β_{OX} relative to the measured spectral slope of the afterglow in the X-ray band. We use the same symbols as used in Fig. 2. The bursts falling in the gray area fulfill the V09 criterion. Here $\beta_{OX} = 0.5$ is highlighted in order to compare with the J04 criterion.

error of 0.5 mag, this would translate into a ∼0.07 systematic error in the upper limit of β_{OX} and an error of 0.5 mag in the extrapolated R_C-band upper limit. Fortunately, in no case did this uncertainty affect our potential classification of a burst as dark.

For the optical/NIR bands, we proceeded as follows. To compare the different bursts, we shifted upper limits to a common band, the R_C band. This required us to know the spectral slope β_{OX}, and a conservative upper limit on it was obtained by taking into account all afterglow upper limits in time and filter. Thereby, if possible, we used only optical upper limits that were taken at times reasonably separated from the prompt GRB phase. Special care was taken when the deepest afterglow upper limits had only been obtained in bands shortwards of R_C. We then chose to use the reddest filter, since the blue part of the spectrum is more affected by both Lyman dropout and uncertainties in extinction than the red part. Among all computed values, we finally chose those that implied the lowest β_{OX} values. The resulting R_C-band upper limits are shown in Fig. 1 and they were used to depict the J04 criterion in Fig. 2.

For the X-rays, we used the flux density at 1.73 keV (corrected for Galactic absorption), which is the logarithmic mean of the *Swift*/XRT window (0.3–10 keV). Where the X-ray data are concerned, we gave priority to time intervals where the light curves were smoothly decaying (which differ from burst to burst) and during which β_X was constant (within the errors).

Table 2 summarizes our results where $\Delta = \beta_X - \beta_{OX} - 0.5$. To be conservative, we used its minimum value Δ_{min}, based on the 90% c.l. error of β_X. If $\Delta_{min} > 0$, a burst is classified as dark according to V09. Five events, namely GRBs 050922B, 070429A, 080207, 080218B, and 080602, are dark according to both definitions, while GRB 050717 is dark according only to J04 and GRBs 080915A and 081204 are only dark according to V09 (Figs. 2, 3). Following the above discussion, we assume that a GRB is dark if it fulfills the criterion of J04 as well as V09.

We note that when the optical upper limits were obtained some shortcomings might have limited the validity of this approach: (1) an X-ray light curve that is rather flat might be indicative of an additional X-ray component, while the aforementioned procedure assumes a single radiation component (this affects GRB 080602), (2) a substantial time gap in the X-ray data base (GRB 050922B), (3) an evolving X-ray spectral slope

Table 2. Summary of the darkness properties of our sample.

#	GRB	Time (s)	UL	Filter	UL_R	Ref.	β_{OX}	β_X	Δ_{min}	Comments
(1)	(2)	(3)	(4)	(5)	(6)	(7)	(8)	(9)	(10)	(11)
1	050717	420	19.0	v	18.2	[1]	<0.40	$0.92^{+0.23}_{-0.22}$	−0.20	a; b
2	050922B	49 000	22.5	r'	22.3	[2]	<0.39	$1.87^{+0.49}_{-0.37}$	0.61	c
3	060211A	19 980	22.0	R_C	21.8	[3]	<0.71	$1.24^{+0.28}_{-0.21}$	−0.18	–
4	060805A	63 000	22.9	r'	22.7	[4]	<1.00	$1.49^{+0.50}_{-0.62}$	−0.63	–
5	060919	918	20.2	v	19.8	[5]	<0.68	$1.10^{+0.53}_{-0.62}$	−0.70	a
6	060923B	295	18.5	v	17.9	[6]	<0.62	$1.28^{+0.59}_{-0.53}$	−0.37	b
7	061102	1480	20.5	v	20.1	[7]	<1.10	$0.84^{+0.74}_{-0.74}$	−1.50	d
8	070429A	44 064	24.0	R_C	23.8	[8]	<0.42	$1.25^{+0.25}_{-0.19}$	0.14	•; g
9	070517	57 600	24.5	i'	24.3	[9]	<0.56	$1.27^{+0.19}_{-0.30}$	−0.09	f
10	080207	5364	20.3	R_C	20.5	[10]	<0.26	$1.50^{+0.19}_{-0.18}$	0.56	•
11	080218B	11 520	24.7	r'	24.3	Table A.3	<0.18	$1.36^{+0.22}_{-0.22}$	0.46	•
12	080602	504	20.3	v	20.2	[11]	<0.05	$1.01^{+0.13}_{-0.12}$	0.34	e
13	080727A	2268	19.8	K	22.8	[12]	<0.85	$1.47^{+0.26}_{-0.17}$	−0.05	–
14	080915A	6840	22.1	I_C	22.1	[13]	<0.62	$2.10^{+1.30}_{-0.90}$	0.08	d
15	081012	69 660	23.5	r'	23.4	Table A.3	<0.83	$0.69^{+0.51}_{-0.47}$	−1.11	–
16	081105	46 224	23.0	r'	22.8	Table A.3	<0.61	$2.10^{+1.70}_{-1.20}$	−0.21	d
17	081204	34 560	24.1	r'	23.9	Table A.3	<0.55	$1.93^{+1.56}_{-0.77}$	0.11	d

Notes. *Columns:* (3 to 5) Time after the burst and reported upper limits (UL) of the afterglow (observed magnitudes); r'-band magnitudes are given in the AB system, all others in the Vega/UVOT system. (6) Deduced UL in the R_C band (AB system) after correcting for Galactic extinction and shifting from the native filter wavelength (Col. 5) to the R_C band using the upper limit to β_{OX}. (8) If $\beta_{OX} < 0.5$, then a burst is dark according to J04. (10) The minimum value (based on the 90% confidence error of β_X) of the quantity $\Delta = \beta_X - \beta_{OX} - 0.5$. If $\Delta_{min} > 0$, then a burst is dark according to V09. (11) (a) During the time of the observed UL the SED in the X-ray band is not constant. (b) The observed UL lies close to the end of the prompt GRB phase. (c) No X-ray data exist for the time when the UL was obtained. (d) Very faint X-ray flux; no well-defined X-ray light curve. (e) Flat X-ray light curve during the time when the UL was obtained. (f) The optical afterglow was detected; see Sect. 3.3. (g) No UL is reported in the corresponding GCN (Price 2007). We used $R_C = 24.0$ based on the original data, which are available in the Gemini archive. A bullet (•) indicates that the burst is truly dark according to J04 and V09 (Sect. 2.3). *Column* (7; references): 1) Blustin et al. (2005); 2) Guziy et al. (2005); 3) Sharapov et al. (2006); 4) Rol & Page (2006); 5) Breeveld & Guidorzi (2006); 6) Holland & Cucchiara (2006); 7) Holland (2006); 8) Price (2007); 9) Fox et al. (2007); 10) Andreev et al. (2008); 11) Beardmore et al. (2008e); 12) Levan & Wiersema (2008); 13) Rossi et al. (2008c).

(GRB 050717), and (4) a large error (>1) in the X-ray spectral slope (GRB 080915A, GRB 081105, and 081204). Taking all this into account, only three events in our sample can be securely classified as dark bursts (GRB 070429A, GRB 080207, and GRB 080218B). All other bursts, except for GRB 070517, may still be truly dark bursts but the available data are insufficient to claim this with certainty.

3. Results

3.1. General

In the following, we report the results of our deep late-time observations for each GRB field. They are summarized in Tables 3–5.

If not stated otherwise, in the following R_C, K_s-band magnitudes, and colors are given in the AB magnitude system, in order to allow for a direct comparison with data of confirmed GRB host galaxies compiled by Savaglio et al. (2009; in the following SBG09), i.e., host galaxies that are identified via optical afterglow detections obtained with sub-arcsec accuracy. All $(R_C - K_s)$ colors were corrected for Galactic extinction, estimated using the extinction maps published by Schlegel et al. (1998). Extinction corrections for the GROND filters are $A(g') = 1.253 A_V$, $A(r') = 0.799 A_V$, $A(i') = 0.615 A_V$, $A(z') = 0.454 A_V$, $A(J) = 0.292 A_V$, $A(H) = 0.184 A_V$, and $A(K) = 0.136 A_V$, while for all other instruments

we assumed the standard values of $A(R_c) = 0.748 A_V$ and $A(K) = 0.112 A_V$ (Rieke & Lebofsky 1985). We always set $A_V = 3.1 E(B − V)$.

3.2. Selecting host galaxy candidates

Even in the case of arcsec-sized error boxes, it is usually difficult to determine the most likely GRB host galaxy candidate. The approach we used here to identify a putative host is identical to the approach adopted 15 years ago, when no afterglows were known at all and at best only arcmin-sized error boxes obtained via satellite triangulation were available (e.g., Vrba et al. 1995; Klose et al. 1996; Schaefer et al. 1998; Vrba et al. 1999). The main observational difference is the size of the XRT error circles provided by *Swift*/XRT that can go down to 1–2 arcsec, allowing meaningful searches for host galaxies.

We analyzed all objects present in an XRT error circle and studied their properties following different criteria in order to establish the best GRB host candidate. The first criterion is the magnitude-probability criterion.

Following Bloom et al. (2002) and Perley et al. (2009), we calculated, for every object, the probability p of finding a galaxy of any type of the given (extinction-corrected) R_C-band magnitude m in a region of radius r, where r is the radius of the associated error circle. It is

$$p(m) = 1 - \exp(-\pi r^2 \sigma(\leq m)), \tag{1}$$

Table 3. Summary of the photometry of all objects found in the XRT error circles based on the VLT observations.

#	GRB	Object	RA, Dec (J2000)	R_{AB}	K_{AB}	UL_R	UL_K	XRTpos
2	050922B	–	no candidates	>26.5	>22.8	26.5	22.8	
5	060919	A	18:27:41.78, −51:00:51.0	26.14 ± 0.24	>23.4	26.5	23.4	1
6	060923B	A[a]	15:52:46.49, −30:54:12.3	23.10 ± 0.11	21.76 ± 0.09	26.6	24.3	2
		B[a]	15:52:46.61, −30:54:10.3	21.67 ± 0.02	18.95 ± 0.03	26.6	24.3	2
		C[a]	15:52:46.56, −30:54:14.6	24.49 ± 0.04	22.87 ± 0.15	26.6	24.3	1
		D[a]	15:52:46.63, −30:54:16.4	25.74 ± 0.12	21.63 ± 0.06	26.6	24.3	2
		E[a]	15:52:46.66, −30:54:12.9	blended with A	blended with A	26.6	24.3	1
7	061102	A	09:53:37.93, −17:01:22.7	24.10 ± 0.06	>22.8	26.9	22.8	2
		B	09:53:37.89, −17:01:30.8	23.96 ± 0.06	>22.8	26.9	22.8	2
8	070429A	A	19:50:48.78, −32:24:13.6	25.01 ± 0.20	22.57 ± 0.25	26.5	23.8	3
		B[a]	19:50:48.78, −32:24:18.1	24.14 ± 0.09	22.39 ± 0.21	26.5	23.8	1
		C[a]	19:50:48.90, −32:24:17.4	24.32 ± 0.08	21.89 ± 0.14	26.5	23.8	1
		D	19:50:49.10, −32:24:17.3	>26.5	23.01 ± 0.40	26.5	23.8	2
9	070517	A	18:30:29.08, −62:17:53.0	25.39 ± 0.21	>23.4	26.6	23.4	1
10	080207	A	13:50:03.03, +07:30:09.3	25.15 ± 0.17	23.02 ± 0.39	26.9	23.6	2
		B	13:50:02.97, +07:30:07.2	26.49 ± 0.37	21.77 ± 0.14	26.9	23.6	1
11	080218B	A	11:51:49.69, −53:05:49.1	26.23 ± 0.13	21.74 ± 0.10	27.3	24.0	1
		B	11:51:50.00, −53:05:47.4	24.62 ± 0.04	22.74 ± 0.24	27.3	24.0	3
12	080602	A	01:16:42.15, −09:13:55.0	22.95 ± 0.02	22.55 ± 0.05	26.9	23.5	1
		B	01:16:42.12, −09:13:57.5	24.00 ± 0.06	>23.5	26.9	23.5	2
		C	01:16:42.14, −09:13:53.4	>26.9	22.49 ± 0.14	26.9	23.5	2
13	080727A	–	no candidates	>26.3	>23.0	26.3	23.0	
14	080915A	A	01:11:47.80, −76:01:13.9	21.63 ± 0.01	20.42 ± 0.02	26.3	23.4	1
		B	01:11:45.27, −76:01:10.4	21.28 ± 0.01	19.19 ± 0.01	26.3	23.4	3
		C[a]	01:11:47.47, −76:01:10.0	24.71 ± 0.07	>23.4	26.3	23.4	1
		D[a]	01:11:46.98, −76:01:09.5	24.57 ± 0.08	>23.4	26.3	23.4	2
		E[a]	01:11:47.16, −76:01:15.1	25.44 ± 0.15	>23.4	26.3	23.4	1
15	081012	A	02:00:48.18, −17:38:15.2	25.16 ± 0.17	>23.9	26.7	23.9	2
16	081105	A	00:15:48.42, +03:28:11.6	23.73 ± 0.08	22.78 ± 0.18	26.1	24.5	1
		B	00:15:48.30, +03:28:13.8	24.34 ± 0.13	22.13 ± 0.14	26.1	24.5	1
		C	00:15:48.46, +03:28:10.7	>25.3	21.74 ± 0.13	26.1	24.5	1
17	081204	A[b]	23:19:09.39, −60:13:31.5	23.21 ± 0.04	22.37 ± 0.16	26.4	24.3	1
		B[a]	23:19:09.13, −60:13:30.2	23.54 ± 0.06	21.59 ± 0.08	26.4	24.3	1
		C	23:19:08.99, −60:13:23.4	23.16 ± 0.07	22.06 ± 0.11	26.4	24.3	2
		D	23:19:08.89, −60:13:37.6	24.19 ± 0.10	22.16 ± 0.15	26.4	24.3	2
		E	23:19:09.10, −60:13:39.4	24.32 ± 0.12	>24.3	26.4	24.3	2
		F[a]	23:19:09.24, −60:13:29.4	24.65 ± 0.50	21.53 ± 0.07	26.4	24.3	1
		G	23:19:08.30, −60:13:39.0	blended with a star	21.57 ± 0.15	26.4	24.3	2

Notes. Column: (2) GRB 050717, GRB 060211A, and GRB 060805A are the only bursts in our sample for which we do not have VLT data (see Table 4). (3) Objects identified in the XRT error circles (see Sect. 3.3). (5) Observed magnitudes. UL stands for the 3σ upper limit. The last column defines the distance of the object from the center of the 90% XRT error circle of radius r_0 (see Table 1). A value n means that the source lies within $[(n-1)r_0, nr_0]$. *Special notes about the photometry:* all magnitudes are based on $(2 \times FWHM)$ aperture photometry, except for cases where the object was affected by near-by objects. In the latter case, we used either [a] PSF photometry or [b] $1 \times FWHM$ aperture photometry . In particular, we gave preference to the latter in the case of elongated objects.

where $\sigma(\leq m)$ is the surface density of galaxies with magnitudes $\leq m$ (Eq. (3) in Bloom et al. 2002). If the object we have found is located within the 90% c.l. XRT error circle of radius r_0, we set $r = r_0$, if it is placed within $[(n-1)r_0, nr_0]$, then we set $r = nr_0$. The input for $\sigma(\leq m)$ is the relation derived by Hogg et al. (1997), which is based on galaxy counts down to about $R_{Vega} = 26.5$. We consider galaxies of all types as very likely GRB host galaxy candidates if the chance probability p

of finding such an object of the given R_C-band magnitude in the corresponding error circle is $\leq 10\%$ (within 1σ).

Other criteria rely on the phenomenological appearance of the galaxies, particularly their color. Spiral galaxies can have a $(R - K)_{AB}$ color as red as about 3.5 mag before the Lyman dropout at high z comes into play (SBG09; their Fig. 3). Galaxies with a redder $(R - K)_{AB}$ color are therefore of special interest, since they can be either dust-enshrouded or Lyman-dropped-out

Table 4. Summary of the photometry of all objects found in the XRT error circles based on observations with GROND.

#	GRB	Obj.	RA, Dec (J2000)	g'_{AB}	r'_{AB}	i'_{AB}	z'_{AB}	J_{AB}	H_{AB}	K_{AB}	XRTpos
1	050717	A	14:17:24.56, −50:31:58.7	>25.4	23.65(10)	23.01(11)	23.40(30)	>22.6	>21.9	>21.1	2
		B[b]	14:17:24.58, −50:32:01.6	>25.4	24.50(40)	23.50(40)	22.80(30)	>22.6	>21.9	>21.1	1
3	060211A	A	03:53:32.66, +21:29:19.8	>25.2	24.51(20)	>24.8	>24.4	>23.4[n]	>21.6	>21.6[n]	1
		B	03:53:32.43, +21:29:16.3	23.60(08)	23.09(06)	22.76(09)	23.31(10)	<23.1[n]	>21.6	21.50(20)[n]	3
		C	03:53:32.57, +21:29:18.0	>25.2	>24.9	>24.8	>24.4	23.10(30)[n]	>21.6	>21.6[n]	1
		D	03:53:32.69, +21:29:20.9	>25.2	>24.9	>24.8	>24.4	23.40(40)[n]	>21.6	>21.6[n]	2
4	060805A	A	14:43:43.49, +12:35:12.5	>25.5	25.4(40)	>24.6	>24.2	>22.9	>21.8	>21.1	1
		B	14:43:43.39, +12:35:10.1	23.42(16)	23.68(12)	>24.6	>24.2	>22.9	>21.8	>21.1	2
10	080207	A-B	see Table 3	>25.4	>24.9	>23.9	>23.8	>22.0	>20.8	>20.1	1,2
11	080218B	A	see Table 3	>25.5	>24.9	>24.2	>24.1	>22.8	>21.4	>21.2	1
		B	see Table 3	25.10(30)	24.30(30)	–	23.27(10)	>22.8	>21.4	>21.2	3
12	080602	A	see Table 3	22.96(10)	22.93(08)	22.86(13)	22.60(14)	>21.4	>21.0	>20.6	1
		B	see Table 3	>25.3	23.73(12)	23.90(29)	22.97(17)	>21.4	>21.0	>20.6	2
		C	see Table 3	>25.3	>25.5	>24.9	>24.6	>21.4	>21.0	>20.6	2
14	080915A	A	see Table 3	22.05(10)	21.27(10)	21.21(10)	20.80(10)	20.53(02)	20.37(03)	20.39(15)	1
		B	see Table 3	23.30(30)	21.14(05)	20.88(06)	20.28(12)	19.74(06)	19.33(06)	19.00(08)	3
		C-E	see Table 3	>24.0	>24.3	>24.1	>23.9	>22.1	>21.3	>21.3	1,2
15	081012	A	see Table 3	>23.8	>23.8	>23.4	>23.2	>21.8	>21.3	>21.0	2
16	081105	A-C	see Table 3	>24.0	>23.9	>23.3	>22.9	>21.4	>20.7	>20.3	1
17	081204	A[b]	see Table 3	23.69(10)	23.74(08)	23.25(11)	23.09(15)	22.50(16)[s]	>21.5	>20.9	1
		B[b]	see Table 3	24.18(30)	23.74(08)	23.53(14)	23.29(17)	22.15(15)[s]	>21.5	>20.9	1
		C	see Table 3	>25.0	23.96(17)	23.62(28)	>24.0	22.55(19)[s]	>21.5	>20.9	2
		D-G	see Table 3	>25.0	>25.0	>24.7	>24.0	>22.0[s]	>21.5	>20.9	1,2

Notes. Columns (4–10): observed magnitudes. Magnitude errors are given in units of 10 mmag. The letters n and s are used to mark those magnitudes resulting from [n] NEWFIRM and [s] NTT/SOFI imaging, respectively. For GRB 080218B/object B the i'-band data are affected by a ghost image from a bright star. Upper limits are 3σ. *Special notes about the photometry:* see Table 3.

galaxies. These galaxies are usually called extremely red objects (EROs) and were first addressed in the context of deep NIR surveys (Elston et al. 1988). Number counts for these galaxies are now available (Gonzalez-Perez et al. 2009; Hempel et al. 2011; Kim et al. 2011) and will be used in the following. Finding an ERO galaxy in an XRT error circle can be considered as strong evidence that this object is related to the burst under consideration.

The ERO galaxy population follows a bimodal distribution and consists of both passively evolving ellipticals and dusty star-forming galaxies in the redshift interval $1 \lesssim z \lesssim 2$ (Doherty et al. 2005; Fontanot & Monaco 2010; Gonzalez-Perez et al. 2011). The ratio of both populations is still a matter of debate (see Conselice et al. 2008; Gonzalez-Perez et al. 2009; Kong et al. 2009; Fontanot & Monaco 2010). Since long GRBs tend to be hosted by star-forming galaxies, the ERO number counts provide a conservative upper limit to the probability of finding a star-forming ERO galaxy in a *Swift*/XRT error circle.

Finally, a close pair of galaxies inside an XRT error circle, i.e., a hint of interaction and thus triggered star-formation, is a good candidate to be the birthplace of a (long) GRB progenitor.

3.3. Notes for individual targets

We now report on the observations and results for each individual target. In several cases, we could make use of late-time as well as early-time GROND or VLT data. However, the comparison between different observing epochs did not reveal any fading afterglows, except for the case of GRB 070517, where a comparison with published Gemini-S data led to the identification of the afterglow.

GRB 050717. The burst occurred at relatively low Galactic latitude ($b = 10°$), and the field is relatively crowded with stars. The foreground Galactic reddening is moderate, $E(B − V) = 0.24$ mag, but the highest in our sample. The 90% c.l. XRT error circle has a radius of $r_0 = 1''.5$.

We observed the field with GROND two years after the burst. Within $2r_0$, two objects (A and B) are visible in the combined $r'i'z'$-band image (Fig. 4). Object A ($r'_{AB} = 23.6$) lies outside $1r_0$, appears fuzzy, and has a size of about $2''.1 \times 3''.9$. On the basis of its visual appearance, this is a faint galaxy. Its outer parts extend into the 90% c.l. error circle. The fainter object B ($r'_{AB} = 24.5$) lies within $1r_0$ close to the southern boundary of the error circle. Neither object is detected in g' and they are also not seen in the NIR bands (Table 4). Given the non-detection in the NIR ($K_{AB} > 21.1$), for both objects only an upper limit to $(R − K)_{AB}$ can be given (<2.1 mag and <2.9 mag, respectively)[7].

Assuming that A and B are galaxies, the probability p of finding a galaxy of the given R_C-band magnitude in a region of radius $2r_0$ and $1r_0$ is about 0.05 and 0.03, respectively[8]. We therefore consider both objects as equally likely GRB host galaxy candidates.

GRB 050922B. This burst occurred at high Galactic latitude ($b = −67°$); the field is not crowded with stars. The foreground Galactic reddening is very small, at $E(B − V) = 0.04$ mag. The

---

[7] Here and in the following, we make the simplifying assumption ($r' − K)_{AB} = (R_C − K)_{AB}$ and write $(R − K)_{AB}$ when we provide (extinction-corrected) colors based on GROND data.

[8] Here and in the following, we set R_C(Vega) = r'(Vega) when calculating p-values based on Eq. (1).
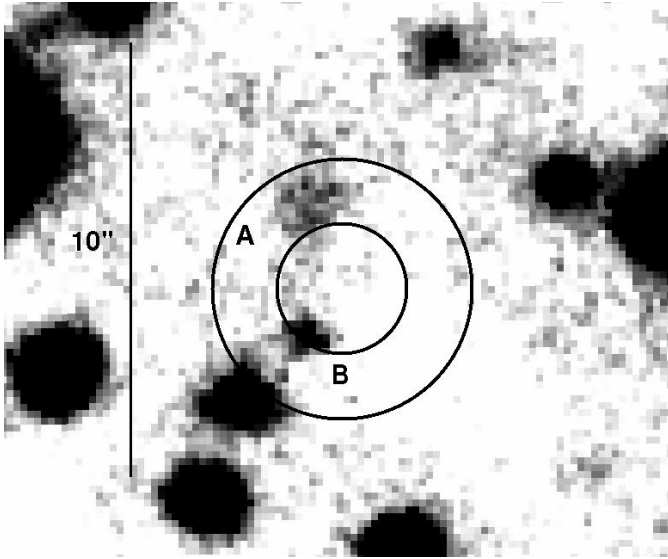
Fig. 4. GROND combined $r'i'z'$-band image of the field of GRB 050717. It shows the 90% c.l. XRT error circle ($r_0 = 1.''5$), as well as a circle of radius $2r_0$. Here and in the following, east is left and north is up.
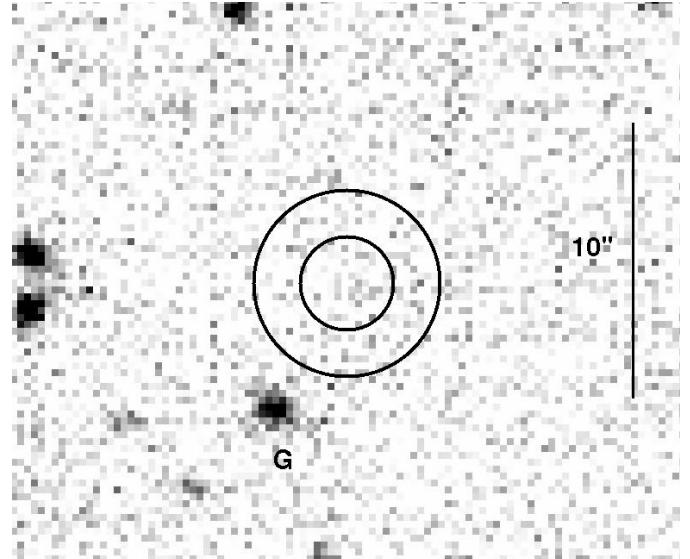

Fig. 5. FORS2 R_C-band image of the field of GRB 050922B. It shows the 90% c.l. XRT error circle ($r_0 = 1.''7$), as well as a circle of radius $2r_0$.

90% XRT error circle has a radius of $r_0 = 1.''7$ (Fig. 5). The field was observed with NEWFIRM in the K_s-band about three years after the burst. Additional data were obtained with FORS2 and ISAAC one year later. No object is found in any band, neither within the 90% c.l. XRT error circle nor within $2r_0$, down to deep 3σ upper limits of $R_{AB} > 26.5$ and $K_{AB} > 22.8$.

GRB 060211A. The field of GRB 060211A lies at relatively low Galactic latitude ($b = -24°$) but is not crowded with stars. The foreground Galactic reddening is moderate, $E(B - V) = 0.19$ mag. The 90% c.l. XRT error circle has $r_0 = 1.''4$.

We observed the field 1.5 and 3 years after the burst with GROND and NEWFIRM (J and K), respectively. In the 90% c.l. error circle, we find one object (A) in the GROND r' band, which looks slightly extended in the north-south direction ($1.''1 \times 1.''2$). The object is not visible in the other GROND bands. Complementary NEWFIRM observations also did not detect this object down to $J_{AB} = 23.4$ and $K_{AB} = 21.6$ (Table 4). Only an upper limit to the $(R - K)_{AB}$ color of object A can therefore be given (<2.5 mag).

In addition to A, an extended, fuzzy object (B) is detected with GROND in $g'r'i'z'$, and located about $4.''0$ ($3r_0$) south-west of the center of the error circle (Fig. 6). This object is also seen in the NEWFIRM J-band image, where it appears resolved into two or three sources. In the r' band, its size is about $3.''8 \times 2.''2$.

The NEWFIRM J-band image reveals an other two very faint sources, C and D. Object C ($J_{AB} \sim 23.1$) is an extended object lying within the 90% c.l. error circle. This potential host galaxy is not seen in any other band. Object D ($J_{AB} \sim 23.4$) lies outside the 90% c.l. error circle and is too faint for us to draw any conclusion about its morphology and nature. The angular offset of D from the boundary of the 90% c.l. error circle is $0.''7$. For a redshift of 0.5 or 1.0, this would correspond to a projected distance of 4.3 kpc and 5.6 kpc, respectively. Compared to the median projected angular offset of 1.3 kpc found by Bloom et al. (2002) for a sample of 20 host galaxies of long bursts, this is a high but still reasonable value for e.g. a Milky Way-like galaxy. In the case of object B, the angular offset

is $2.''5$, corresponding to a projected distance of 15 kpc and 20 kpc, respectively, which most likely excludes object B as a host galaxy candidate. Unfortunately, we cannot decide whether objects C and D are potential ERO galaxies. An ERO would have an $(r' - J)_{AB}$ color of at least 2 mag, but our detection limit is insufficiently deep to check this out. Assuming that A is a single galaxy, the probability p of finding a galaxy of the measured r'-band magnitude within the 90% c.l. error circle is about 0.03, while the corresponding value for object B is 0.08. We conclude that in this case we cannot decide the most likely host galaxy candidate among A, C, or D.

GRB 060805A. The field lies at relatively high Galactic latitude ($b = 60°$). It is not crowded with stars but located close to a bright star ($R_C = 13.5$) at RA, Dec (J2000) = 14:43:42.098, +12:35:20.63 (USNO-B1 catalog), which may affect the background estimation. The foreground Galactic reddening is small, $E(B - V) = 0.02$ mag, among the smallest in our sample. The corresponding 90% c.l. XRT error circle has $r_0 = 1.''6$.

The field was observed with GROND two years after the burst. In the r'-band image, we detect two sources (A, B; Fig. 7) within radii of $1r_0$ and $2r_0$ with magnitudes $r' = 25.4$ and 23.7, respectively. Both objects appear extended. Object B, with a size of $2.''7 \times 1.''3$, lies about $2.''0$ away from the center of the XRT error circle but its outer regions extend into it. In contrast to object A, object B is also detected in the g'-band ($\sim$23.4) with a $(g' - r')_{AB}$ color consistent with a flat SED in this wavelength region. This could imply that this galaxy is dominated by a young stellar population. Both objects are not detected in the GROND $i'z'JHK_s$ bands, where only deep upper limits could be derived (Table 4). The $(R - K)_{AB}$ colors of A and B are <4.3 mag and <2.5 mag, respectively.

Assuming that A and B are galaxies, the probability p of finding a galaxy of the measured R_C-band magnitude within $1r_0$ and $2r_0$, respectively, is about 0.09 for object A and 0.09 for object B. We consider both, A and B, to be GRB host galaxy candidates. The same conclusion was drawn by Perley et al. (2009), who observed this field in g' and R_C using the Keck telescopes.
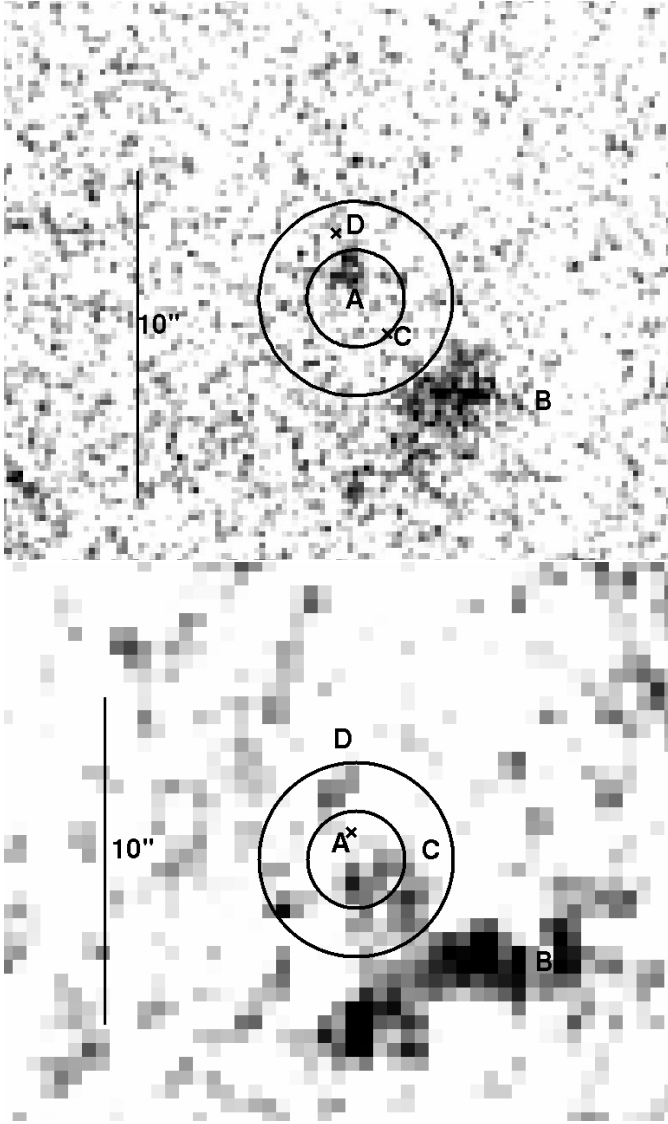
Fig. 7. GROND r'-band image of the field of GRB 060805A. It shows the 90% c.l. XRT error circle ($r_0 = 1''\!.6$), as well as a circle of radius $2r_0$.

Fig. 6. GROND r'-band (*top*) and NEWFIRM J-band image (*bottom*) of the field of GRB 060211A. It shows the 90% c.l. XRT error circle ($r_0 = 1''\!.4$) as well as a circle of radius $2r_0$. The cross in the GROND image indicates the position of objects C and D (only visible in J-band), while a cross in the NEWFIRM image indicates the position of object A (detected only in the optical bands).

Fig. 8. FORS1 R_C-band image of the field of GRB 060919. It shows the 90% c.l. XRT error circle ($r_0 = 1''\!.7$), as well as a circle of radius $2r_0$.

GRB 060919. The field of this burst lies at low Galactic latitude ($b = -17°$) but is not crowded with stars. The foreground Galactic reddening is small, $E(B - V) = 0.07$ mag, and the 90% c.l. XRT error circle is among the smallest in our sample ($r_0 = 1''\!.7$).

The field was observed with FORS1 and ISAAC about two years after the burst in R_C and K_s, respectively. We find only a single R_C-band source within the 90% c.l. error circle (object A; Fig. 8), with $R_{AB} = 26.1$. No other objects are visible even within $2r_0$. In the R_C-band image, object A seems to be extended along the east-west direction ($1''\!.5 \times 1''\!.4$). It is undetected in the ISAAC image down to deep flux limits ($K_{AB} > 23.4$). Its $(R - K)_{AB}$ color is thus <2.6 mag, well within the range of the colors of the known GRB host galaxy population (SBG09). If this object is not the host, then we can provide upper limits for the GRB host galaxy of $R_{AB} > 26.5$ and $K_{AB} > 23.4$.

The probability of finding a galaxy of the measured R_C-band magnitude in a region of radius $1r_0$ is 0.15. Given that object A
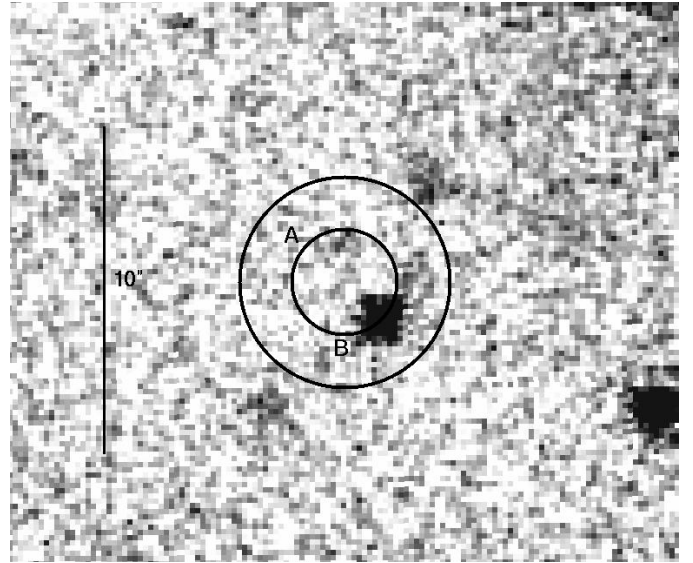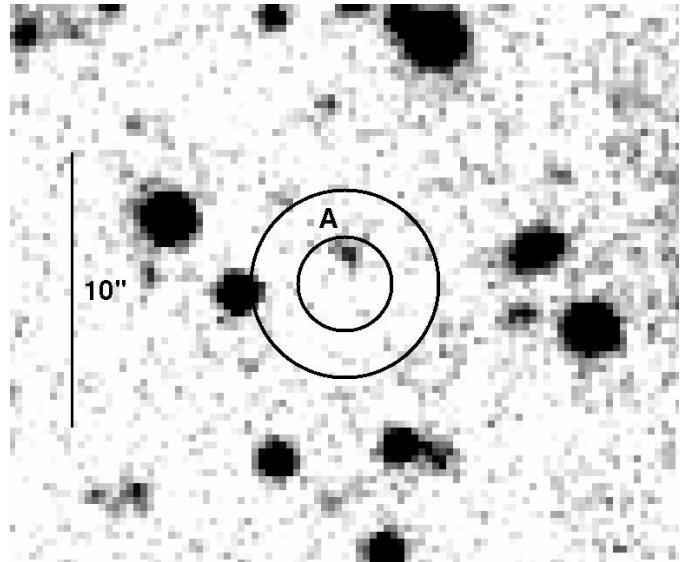
is the only object we detect within $2r_0$, we suggest that it is the potential GRB host galaxy.

GRB 060923B. The field lies at relatively low Galactic latitude ($b = 18°$) and is relatively crowded with bright stars. The foreground Galactic reddening is moderate, at $E(B - V) = 0.15$ mag. The corresponding 90% c.l. XRT error circle has $r_0 = 1''\!.8$.

We observed the field with FORS1 and ISAAC about 1.5 years after the burst. Our FORS1 R_C-band as well as our ISAAC K_s-band observations show two objects (E and C; Fig. 9) at the inner border of the 90% c.l. error circle, while three more objects (A, B, and D) lie within $2r_0$.

Objects A ($R_{AB} = 23.1$) and E are very close to each other, making it difficult to get a reliable R-band photometry, especially for object E. Object B ($R_{AB} = 21.7$) has a PSF that is point-like. In the deep K_s-band image, object A shows an extended morphology ($2''\!.2 \times 2''\!.1$). Object C ($R_{AB} = 24.5$) has a point-like
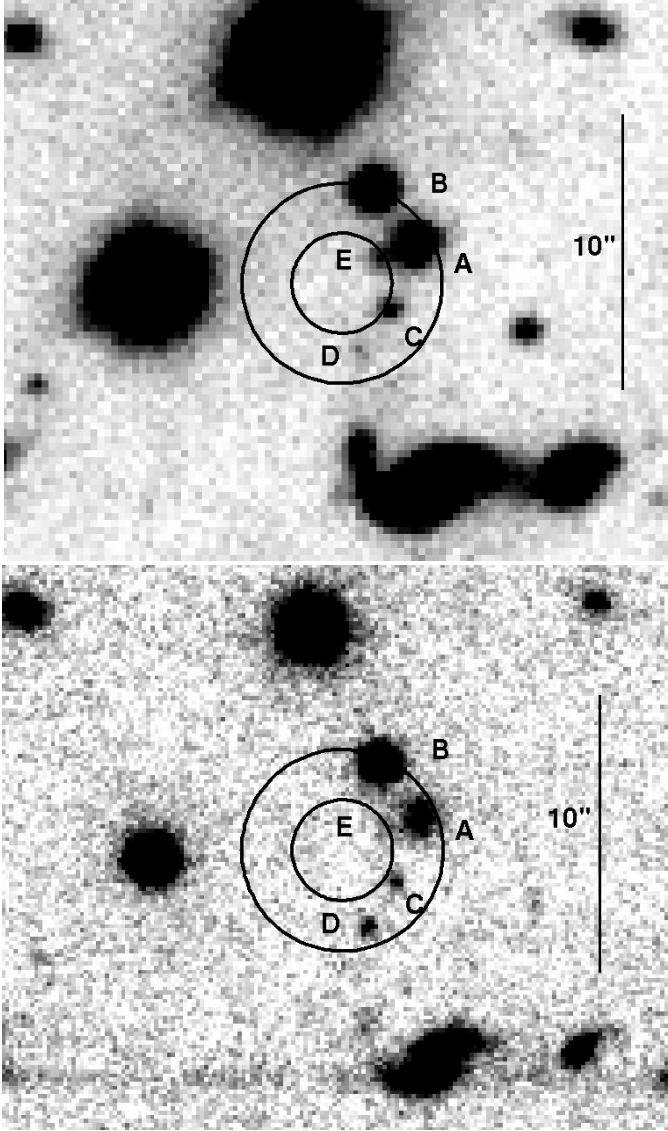
Fig. 9. FORS1 R_C-band (*top*) and ISAAC K_s-band image (*bottom*) of the field of GRB 060923B. Also shown is the 90% c.l. XRT error circle ($r_0 = 1\farcs8$), as well as a circle of radius $2r_0$. The image reveals that object A is a galaxy. Object D is an ERO.

PSF but is probably too faint for detecting the faintest region of a galaxy. Object D appears slightly elongated in the optical and the NIR images, but it is too faint for us to make any conclusion about its morphology. Therefore, with high confidence only object A can be identified as a galaxy.

The probability p of finding a galaxy like A of the measured R-band magnitude within a region of radius $2r_0$ is 0.06. Objects C and E have p-values of less than[9] 0.1, but it is difficult to conclude anything about their nature. If E were a galaxy this would be extremely interesting, because of its position close to galaxy A, which is indicative of a possible interaction. On the other hand, object D ($R_{AB} = 25.7$) is an ERO with $(R - K)_{AB} \sim 3.8$ mag, while A and C have moderately blue colors of 1.1 mag and 1.3 mag, respectively.

Given the results mentioned above, we consider A, C, D, and E as host galaxy candidates.

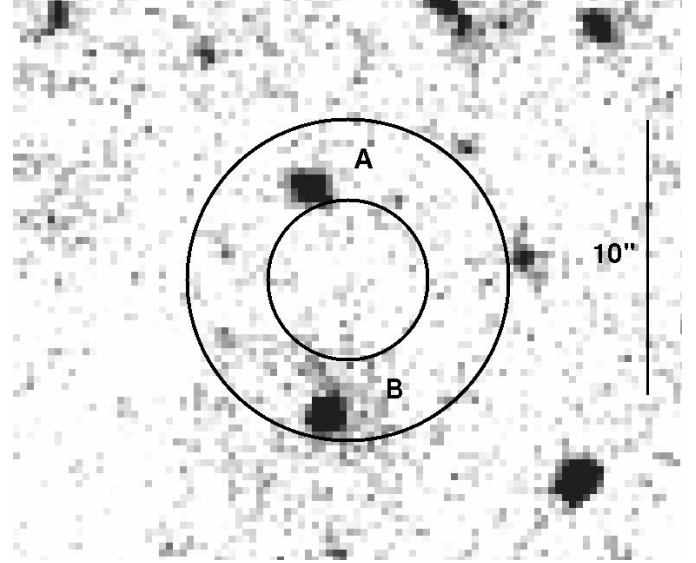[9] Assuming for E a conservative $R = 24.5 \pm 0.5$ gives $p = 0.05 \pm 0.02$.

Fig. 10. FORS1 R_C-band image of the field of GRB 061102. It shows the 90% c.l. XRT error circle ($r_0 = 2\farcs9$), as well as a circle of radius $2r_0$.

GRB 061102. The field lies at moderate Galactic latitude ($b = 28°$). The foreground Galactic reddening is small, $E(B - V) = 0.04$ mag. The corresponding 90% c.l. XRT error circle has a radius of $r_0 = 2\farcs9$.

We observed the field with FORS1 and ISAAC in R_C and K_s, respectively, about 1.5 years after the burst. The VLT images show no object within the 90% c.l. error circle down to $R_{AB} = 26.9$ and $K_{AB} = 22.8$. Two objects (A, B) are found within $2r_0$ (Fig. 10)[10]. They are only detected in R_C but not in K_s. Both objects are clearly extended ($2\farcs5 \times 1\farcs5$ and $1\farcs8 \times 1\farcs9$, respectively). Their $(R - K)_{AB}$ color ($\lesssim 1.2$ mag and $\lesssim 1.1$ mag, respectively) matches the corresponding color of the GRB host galaxy population at a redshift of around $z = 1$ (SBG09). In both cases, the probability of finding a galaxy of the given R_C-band magnitude inside a region of $2r_0$ is 0.3.

Object A touches the 90% c.l. error circle, while the brightness center of object B lies $2\farcs0$ away. However, B is surrounded by a faint, asymmetric halo structure, which extends down to $1r_0$. We speculate that this could be either a face-on spiral galaxy or the tidal tail of an interacting system. If B lies at a redshift of, say, $z = 0.3$ or 0.5, the projected offset of the afterglow from the center of this galaxy would be 9 kpc and 12 kpc, respectively. This is a very large offset. It might be smaller if the redshift were significantly lower, which would then point to a rather subluminous galaxy (see also Sect. 4.6 and Table A.2).

If none of these sources is were the host galaxy, then the measured deep R_C and K_s-band upper limits would make the host galaxy of GRB 061102 one of the faintest in our sample.

GRB 070429A. The field lies at moderate Galactic latitude ($b = -26°$). It is not crowded with stars. The foreground Galactic reddening is modest, at $E(B - V) = 0.17$ mag. The corresponding 90% c.l. XRT error circle has $r_0 = 2\farcs1$.

We observed the field with FORS1 and ISAAC about one year after the burst. In the FORS1 R_C-band image (Fig. 11), we find one object (A) between $2r_0$ and $3r_0$ and two other sources

---

[10] The enhanced 90% c.l. XRT error circle (Evans 2011a,b) includes only object B. Its size is however $5\farcs7$, which is twice as large as the error circle derived by Butler (2007).

within the 90% c.l. error circle (B,C), with R_C-band magnitudes of $25.0 \pm 0.2, 24.1 \pm 0.1$, and 24.3 ± 0.1, respectively. In the ISAAC K_s-band images, another object (D) is marginally visible between $1r_0$ and $2r_0$ ($K_s = 23.0 \pm 0.4$; Fig. 11). All four objects are extended (between $1''7$ and $3''8$ in their major axis). Objects B and C may be an interacting pair because they have a fuzzy structure. The individual R_C, K_s magnitudes of objects A, B, and C (Table 3) and their $(R - K)_{AB}$ colors (Table 5) are compatible with the GRB host population at a redshift $z < 2$ (SBG09). Therefore, the observed colors of objects A, B, and C does not characterize any of them as very red. However, object D is very red ($(R - K)_{AB} > 3.2$ mag). Even though D has a large 0.4 mag error in the K_s-band photometry, we consider it as a potential ERO galaxy. Its center lies outside $1r_0$, but its outskirts reach into the 90% c.l. error circle.

The probability-magnitude criterion gives the following numbers for the first three galaxies (A–C): 0.54, 0.04, and 0.05, respectively. Given that B and C are located within the 90% c.l. error circle, have low p-values, and are probably an interacting galaxy system, we consider both galaxies as equally likely host galaxy candidates. In addition, D is also a host galaxy candidate given its very red color.

GRB 070517A. This burst is unique in our sample, because we could identify its afterglow by comparing our late-time observations with the follow-up observations reported by Fox et al. (2007).

We observed the field with FORS1 and ISAAC about one year after the burst. The field is at a relatively low Galactic latitude ($b = -21°$) but is not very crowded with stars. The foreground Galactic reddening is modest, $E(B - V) = 0.15$ mag. The corresponding 90% c.l. XRT error circle has $r_0 = 2''1$ (Fig. 12).

In the R_C-band image, we detect only one object (A) within the 90% c.l. XRT error circle with magnitudes $R_{AB} = 25.39 \pm 0.21$ and $K_{AB} > 23.4$. No additional objects are apparent within $2r_0$. In particular, we do not detect the $r' = 22.1$ afterglow candidate at RA, Dec (J2000) = 18:30:29.12, −62:17:50.7 (uncertainty of $<0''75$ in each coordinate), which was reported by Fox et al. (2007) based on Gemini-South observations about 16 h after the burst (indicated by a cross in Fig. 12). We conclude that this was the GRB afterglow.

The coordinates of object A agree with the second object detected by Fox et al. (2007) at RA, Dec (J2000) = 18:30:29.08, −62:17:53.0 with $i' = 24.5$. On the basis of our images, we conclude that A is a galaxy. Its angular size is $1.6'' \times 1.3''$, which is about two times larger than the stellar FWHM. If it is the GRB host galaxy, then its $(R - K)_{AB}$ color of <1.7 mag is compatible with the GRB host galaxy population at a redshift around $z = 1$ (SBG09). No underlying galaxy is found at the position of the optical afterglow down to $R_{AB} = 26.6$ and $K_{AB} = 23.4$.

The angular distance between the afterglow and object A is $1''6 \pm 0''3$. The probability p of finding a galaxy of the given R_C-band magnitude in a circle with this radius is between 0.04 and 0.10. If A were the host galaxy of GRB 070517, then its angular distance would translate into a projected distance of 12.8 ± 2.4 kpc, assuming a redshift of $z = 1$. This is ten times larger than the median projected angular offset of 1.3 kpc found by Bloom et al. (2002) for a sample of 20 host galaxies of long bursts, suggesting that object A is not the host. On the other hand, if we require a projected angular distance of less than 10 kpc, then the upper limit on the redshift of this galaxy is $z = 0.4$. In this case, A would be a very faint galaxy relative to the sample of SBG09. Alternatively, the true host galaxy could
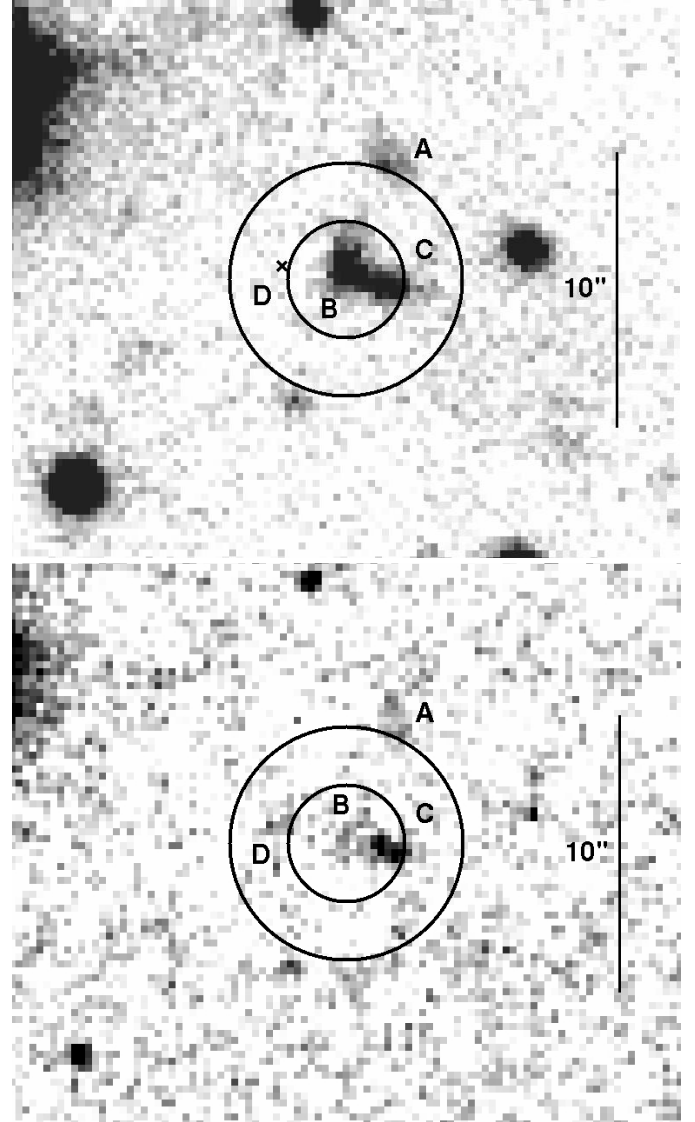

Fig. 11. FORS1 R_C-band image (*top*) and ISAAC K_s-band image (*bottom*) of the field of GRB 070429A. Also shown is the 90% c.l. XRT error circle ($r_0 = 2''1$) as well as a circle of radius $2r_0$. Object D is an ERO. It is not visible in the R_C-band image, where it is indicated by a cross.

coincide with the optical afterglow position but be fainter than our detection limits. We conclude that we are unable to identify a good host galaxy candidate for GRB 070517.

GRB 080207. The burst occurred at high Galactic latitude ($b = 66°$), in a field that is not crowded with stars. The Galactic reddening is very small, at $E(B - V) = 0.02$ mag. The 90% c.l. XRT error circle is the smallest of our sample ($r_0 = 1''4$).

We observed the field two years after the burst, with VLT/VIMOS in R_C and ISAAC in K_s. In addition, deep GROND imaging was performed at a mean time of ten hours after the burst, but no afterglow was detected (Table A.3). Our deep VIMOS R_C-band image shows one fuzzy object of dimensions $2''4 \times 1''3$ at the northeast boundary of the 90% c.l. error circle (A, Fig. 13). This object is very faint in the K_s-band. In addition, the ISAAC image shows another, elongated source (B; $1''6 \times 0''9$) within the XRT error circle that has a very faint R_C-band counterpart with $R_{AB} \sim 26.5$. On the GROND images we
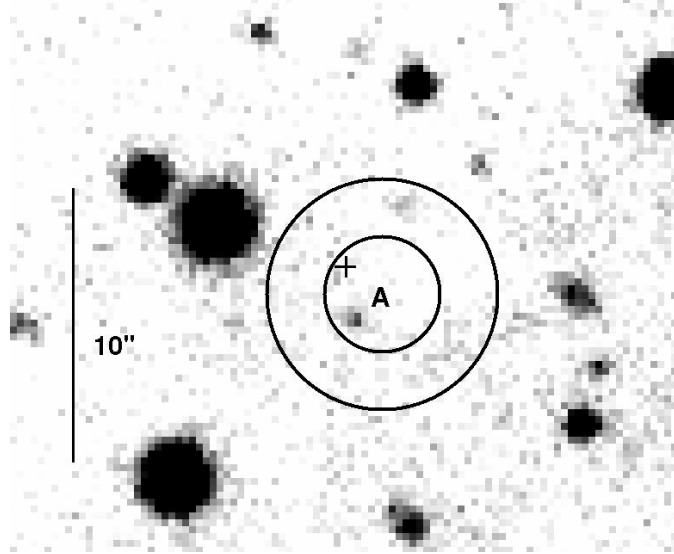
Fig. 12. FORS1 R_C-band image of the field of GRB 070517. It shows the 90% c.l. XRT error circle ($r_0 = 2\rlap{.}''1$), as well as a circle of radius $2r_0$.

do not detect these sources in any band, only upper limits can be provided (Table 4). Object B is very red, $(R - K)_{AB} \sim 4.7$ mag. Its color and morphology defines it as an ERO galaxy. Given its position within the 90% c.l. error circle, we consider B as the most likely GRB host candidate.

As this paper was being finalized, the *Chandra* source catalogue (Evans et al. 2010) became public. Inspection of the catalogue shows that a X-ray observation of the field was performed 8 days after the burst and a point source was detected (CXO J135002.9+073007) at coordinates RA, Dec (J2000) = 13:50:02.97, 07:30:07.8 ($\pm0\rlap{.}''6$). The position of this source is within 1σ consistent with the position of object B. Therefore, we conclude that this is the host galaxy of GRB 080207. Hunt et al. (2011) derived a photometric redshift of about 2.2 for this galaxy, which was subsequently confirmed spectroscopically ($z = 2.086$; Krühler et al. 2012).

GRB 080218B. The field is at a relatively low Galactic latitude ($b = 9°$), the lowest of our sample. However, it is only moderately crowded with stars. The Galactic reddening along the line of sight is modest, at $E(B - V) = 0.17$ mag. The 90% c.l. XRT error circle has a radius of $r_0 = 1\rlap{.}''6$.

We observed the field with FORS2 and ISAAC about one year after the burst. In addition, deep GROND imaging was performed at a mean time of about 0.75 h after the burst, but no afterglow was detected (Table A.3). Our deep FORS2 R_C-band image reveals one faint ($R_{AB} = 26.2$), extended object (A) within the 90% c.l. error circle and another object (B; $R_{AB} = 24.6$) inside $3r_0$. Both objects are also detected with ISAAC at magnitudes $K_{AB} = 21.7$ and 22.7, respectively (Fig. 14). Object A is too faint to be detected by GROND, while B is detected in $g'r'z'$ (Table 4; it is not seen in i' owing to ghost images in the field).

In the FORS image, object A is elongated in the southwest-northeast direction ($2\rlap{.}''5 \times 1\rlap{.}''1$). It could be a spiral galaxy seen nearly edge-on or a tight pair of galaxies. If it is a single galaxy, then its large $(R - K)_{AB}$ color (4.2 mag) defines it as an ERO galaxy. The probability of finding a galaxy of this R_C-band magnitude within an area of radius $1r_0$ on the sky is about 0.1. Given its extremely red color and its position inside the 90% c.l. error circle, we consider A as the most likely GRB host galaxy.
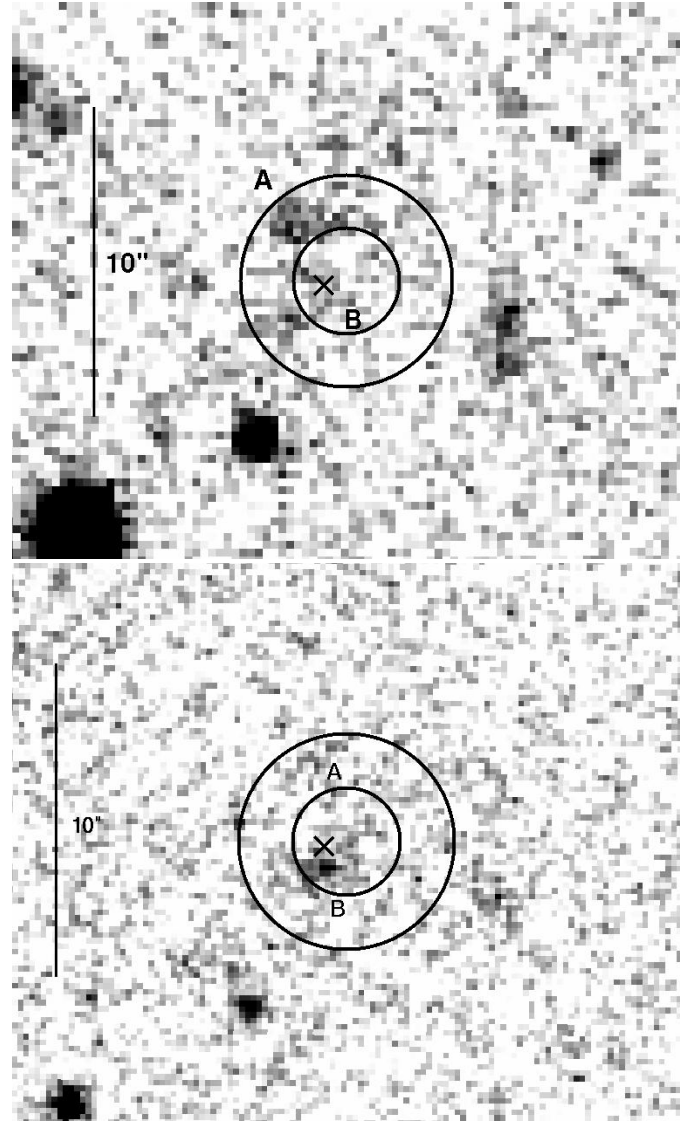
Fig. 13. VIMOS R_C-band (*top*) and ISAAC K_s-band image (*bottom*) of the field of GRB 080207, including the 90% c.l. XRT error circle ($r_0 = 1\rlap{.}''4$), as well as a circle of radius $2r_0$. Object A is only visible in the VLT/VIMOS R_C-band image. Also indicated by a cross is the position of the *Chandra* X-ray source. Object B is an ERO.

GRB 080602. The field is at high Galactic latitude ($b = -71°$), among the highest in our sample. The Galactic reddening is very small, at $E(B - V) = 0.03$ mag. The 90% c.l. XRT error circle has $r_0 = 1\rlap{.}''7$.

We retrieved VLT/FORS2 and ISAAC data obtained about one year after the burst from the ESO archive (program ID 081.A-0856; PI: P. Vreeswijk). In addition, deep GROND multi-color imaging was performed 1.5 years after the burst. In the FORS2 R_C-band image, we find one object (A; $R_{AB} = 22.9$) inside the 90% c.l. error circle. It is also detected in all GROND optical bands and also seen in the ISAAC K_s-band image ($K_{AB} = 22.5$), where it seems to split into two objects, with the second one (C) being $1\rlap{.}''3$ north of A (Fig. 15). Even though in the FORS image, object A looks extended in the northern direction, C has no direct optical counterpart: the angular distance between A and C on the ISAAC image is larger by about $0\rlap{.}''5$ than the distance between the brightness center of A and its fainter northern blob on the FORS image. Therefore, we consider C as a separate object. Its $(R - K)_{AB}$ color (>4.3 mag) defines it as an ERO.
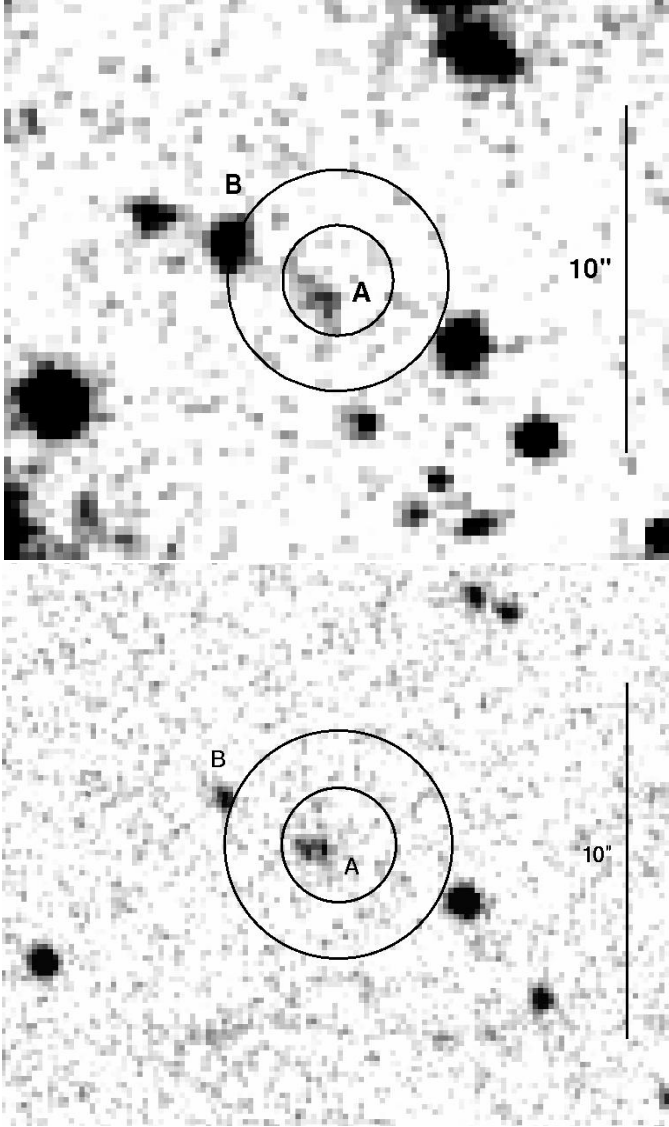
Fig. 14. FORS2 R_C-band image (*top*) and ISAAC K_s-band image (*bottom*) of the field of GRB 080218B, including the 90% c.l. XRT error circle ($r_0 = 1.''6$), as well as a circle of radius $2r_0$. Object A is an ERO.

Fig. 15. FORS2 R_C-band image (*top*) and ISAAC K_s-band image (*bottom*) of the field of GRB 080602, including the 90% c.l. XRT error circle ($r_0 = 1.''7$), as well as a circle of radius $2r_0$. Object C is an ERO. The crosses indicate the positions of objects A and B in the FORS image.

At the southern boundary of the 90% c.l. error circle lies another object (B; size $2.''0 \times 1.''8$), which is possibly another galaxy. In both R_C and K_s-band images, object A looks fuzzy and extended ($2.''6 \times 2.''0$), while the nature of C is less obvious. Assuming that A (including its northern blob) is a single galaxy, a fit of its SED with *Hyperz* (Bolzonella et al. 2000) gives good solutions for both a spiral galaxy with no intrinsic extinction at a redshift of $z = 1.40^{+0.30}_{-0.15}$ (χ^2/d.o.f = 0.074), and a starburst galaxy at a redshift of $z = 2.10^{+0.20}_{-0.35}$ with a moderate Milky Way (MW) extinction of $A_V = 0.4$ mag (χ^2/d.o.f = 0.050; Fig. 16). This twofold solution is due to the SED being fit equally well by a 2175 Å absorption feature or a 4000 Å Balmer jump in the z'-band. We caution, however, that while the first solution implies an absolute magnitude $M_B \sim -23.0$, in the case of the $z \sim 2.1$ solution we obtain $M_B \sim -24.0$, which is very unlikely when compared to the luminosity function found in the Las Campanas redshift survey (Lin et al. 1996). Therefore, we consider $z = 1.4^{+0.30}_{-0.15}$ as the most likely redshift estimation.

Objects A and B have colors $(R - K)_{AB} = 0.3$ mag and <0.4 mag, respectively, which is well within the range of the
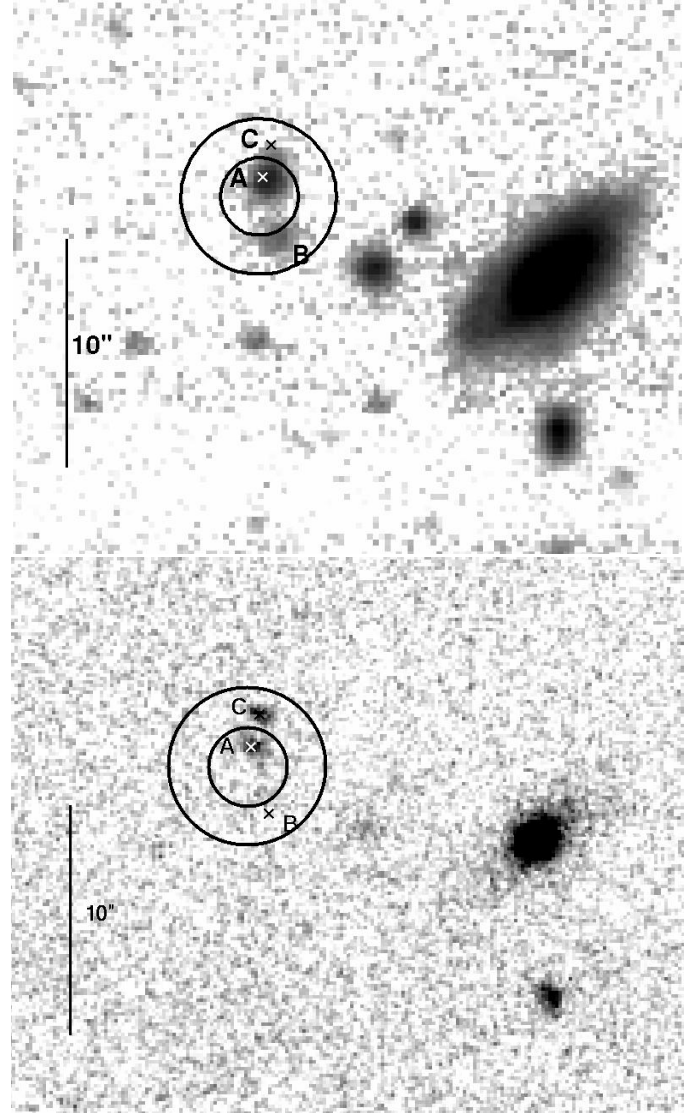
observed colors for GRB host galaxies (SBG09). In the case of object A, the probability of finding a galaxy of the given R_C-band magnitude inside a circular area of radius $1r_0$ is 0.01, while for B the corresponding value is 0.13 (within $2r_0$). However, the probability of finding an ERO (object C) within the same area is much smaller (see Sect. 4.8). Therefore, we consider object C as well as its (possibly interacting) partner A as the most likely host galaxy candidates.

GRB 080727A. The field lies at moderate Galactic latitude ($b = 42°$) and is not crowded by stars. The Galactic reddening is very small, at $E(B - V) = 0.07$ mag. The 90% c.l. XRT error circle has $r_0 = 1.''6$.

We observed the field with ISAAC about 1.5 years after the burst. The deep FORS1 R_C-band image was taken from the ESO archive (program ID 081.A-0856; PI: P. Vreeswijk; FWHM of $0.''8$). No GRB host galaxy is detected within $2r_0$, down to $R_{AB} = 26.3$ and $K_{AB} = 23.0$. This is the second case (besides GRB 050922B) in our sample where only deep upper limits can
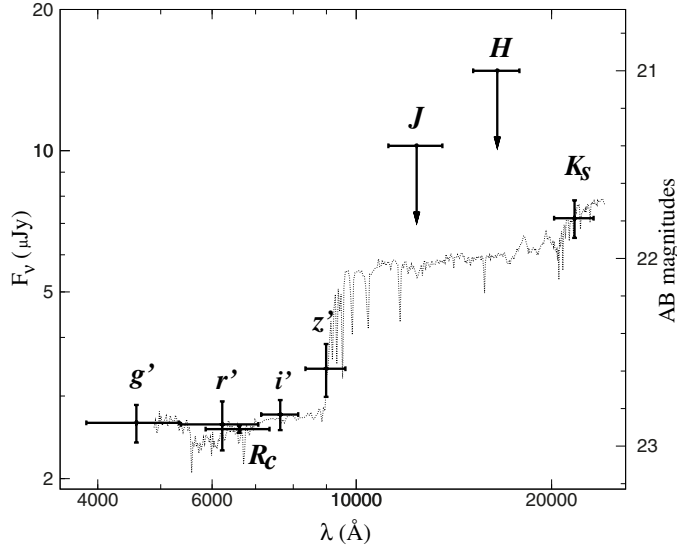
Fig. 16. *Hyperz* best-fit solution of the broad-band SED of object A in the XRT error circle of GRB 080602 (Tables 3 and 4). From left to right: GROND g', GROND r', FORS2 R_C, GROND i', GROND z', GROND J, GROND H, and ISAAC K_s. The best fit corresponds to a spiral galaxy at a redshift of $z = 1.40^{+0.30}_{-0.15}$ with no intrinsic extinction (χ^2/d.o.f = 0.074).
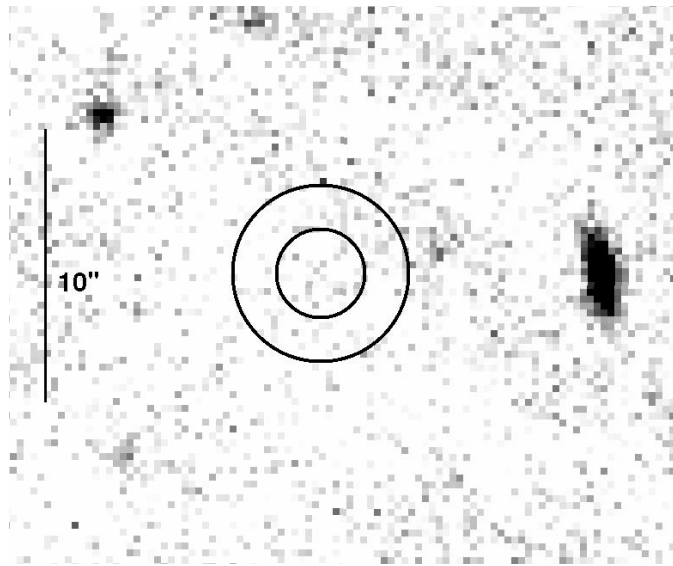

Fig. 17. FORS1 R_C-band image of the field of GRB 080727A. It shows the 90% c.l. XRT error circle ($r_0 = 1\farcs6$), as well as a circle of radius $2r_0$.

Fig. 18. Deep VLT/FORS1 R_C-band (*top*) and HAWKI K_s-band image (*bottom*) of the XRT error circle of GRB 080915A taken 28 h after the burst. Also shown is the 90% c.l. XRT error circle ($r_0 = 3\farcs7$), as well as a circle of radius $2r_0$. In the K_s-band image, object E is not visible and, therefore, is indicated by a cross. Note that all objects visible in the ISAAC image have a counterpart in the FORS1 image taken 11 days later.

be provided for the GRB host galaxy within $2r_0$. A moderately bright, nearly edge-on galaxy ($R_{AB} = 23.4$; size $4\farcs5 \times 2\farcs0$) lies $10''$ west of the center of the XRT error circle. This object lies too far away from the XRT error circle to be physically related to the GRB.

GRB 080915A. The field does not lies at low Galactic latitude ($b = -41°$), but it is relatively crowded with stars. The Galactic reddening is very small, at $E(B - V) = 0.05$ mag. The 90% c.l. XRT error circle is of median size ($r_0 = 3\farcs7$).

The field was observed in the K_s-band with HAWK-I in target of opportunity mode starting 28 h after the burst, lasting for 14 min. No candidate NIR afterglow was found within $2r_0$ down to $K_{AB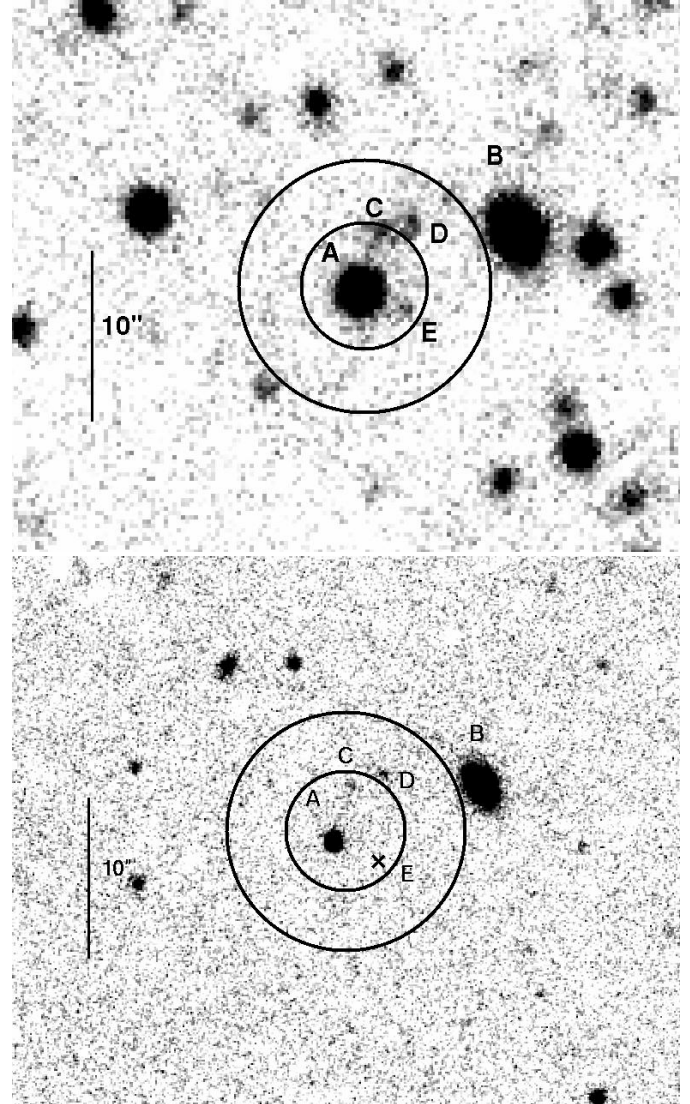} = 23.4$. The HAWK-I observations reveal two bright objects, one (A) within the 90% c.l. error circle and one (B) just outside $2r_0$ with AB magnitudes $K_{AB} = 20.42 \pm 0.02$ and 19.19 ± 0.01, respectively (Fig. 18). These objects were also detected with GROND in all bands during the same night (Table 4). Additional R_C-band data were obtained with FORS1 12 days after the burst (FWHM of $1\farcs4$). The FORS image shows objects A ($R_{AB} = 21.63 \pm 0.01$) and B ($R_{AB} = 21.28 \pm 0.01$), but also reveals the presence of three additional objects: C ($R_{AB} = 24.71 \pm 0.07$) and E ($R_{AB} = 25.44 \pm 0.15$) within $1r_0$, as well as D ($R_{AB} = 24.57 \pm 0.08$) slightly outside $1r_0$.

In the FORS image, object A has a PSF that is compatible with a point source, while C and D appear fuzzy and could be galaxies. Object E is very faint, close to the detection limit. It is difficult to decide whether it is a galaxy. Object B, which is just outside $2r_0$, is a galaxy ($5\farcs6 \times 4\farcs5$ in the FORS1 image) with a relatively large $(g' - r')_{AB}$ color of 2.1 mag.
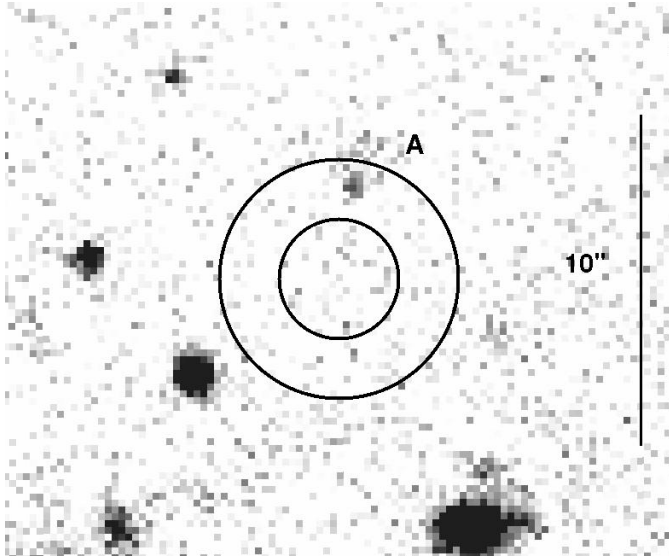
Fig. 19. VIMOS R_C-band image of the field of GRB 081012. It shows the 90% c.l. XRT error circle ($r_0 = 1''8$), as well as a circle of radius $2r_0$.

For objects C and D, the probability of finding a galaxy with the corresponding R_C-band magnitude inside a circle of radius $1r_0$ and $2r_0$ on the sky is $p = 0.23$ and 0.61, respectively. For object E, the probability of finding a galaxy inside a circle of radius $1r_0$ is 0.37. Given that C and D could be an interacting pair, which partly extends into the 90% c.l. error circle, we consider both as GRB host galaxy candidates. If object E is a galaxy, it is the only one well within $1r_0$, thus we also consider E as a host galaxy candidate.

GRB 081012. The field is at high Galactic latitude ($b = -71°$) and is not crowded with stars. The Galactic reddening is very small, at $E(B - V) = 0.02$ mag, among the lowest in our sample. The 90% c.l. XRT error circle has $r_0 = 1''8$.

We observed the field with VIMOS and ISAAC about one year after the burst. Our deep VIMOS R_C-band image shows no source within the 90% c.l. error circle down to $R_{AB} = 26.7$. One object (A, Fig. 19) is detected between $1r_0$ and $2r_0$. It has a cometary shape ($1''8 \times 1''5$) and a magnitude of $R_{AB} = 25.16 \pm 0.17$. It is possible that this is an irregular galaxy or a galaxy with a Galactic foreground star superposed on its southern part. The object is not visible in our ISAAC image down to $K_{AB} = 23.9$. This yields an upper limit of $(R - K)_{AB} < 1.2$ mag, but given the potential foreground star, this color should be considered with caution. The field was also observed by GROND while searching for the afterglow at a mean time of 19.3 h after the burst. Neither object A nor any transient source were detected in any band (Filgas et al. 2008; Tables 4, A.3).

Given the absence of any other source within the 90% c.l. error circle, object A ($p = 0.3$) is the only host galaxy candidate, even though it is a weak candidate: The angular offset of A from the boundary of the 90% c.l. error circle is $1''0$. For a redshift of $z = 1$ or 0.5, this would correspond to a projected distance of 8.0 kpc and 6.0 kpc, respectively. This is a relatively large value (Bloom et al. 2002). If object A is not the host, then the GRB host galaxy is fainter than $R_{AB} = 26.7$ and $K_{AB} = 23.9$.

GRB 081105. The field is at a moderately high Galactic latitude ($b = -58°$) that is not very crowded by stars. The Galactic
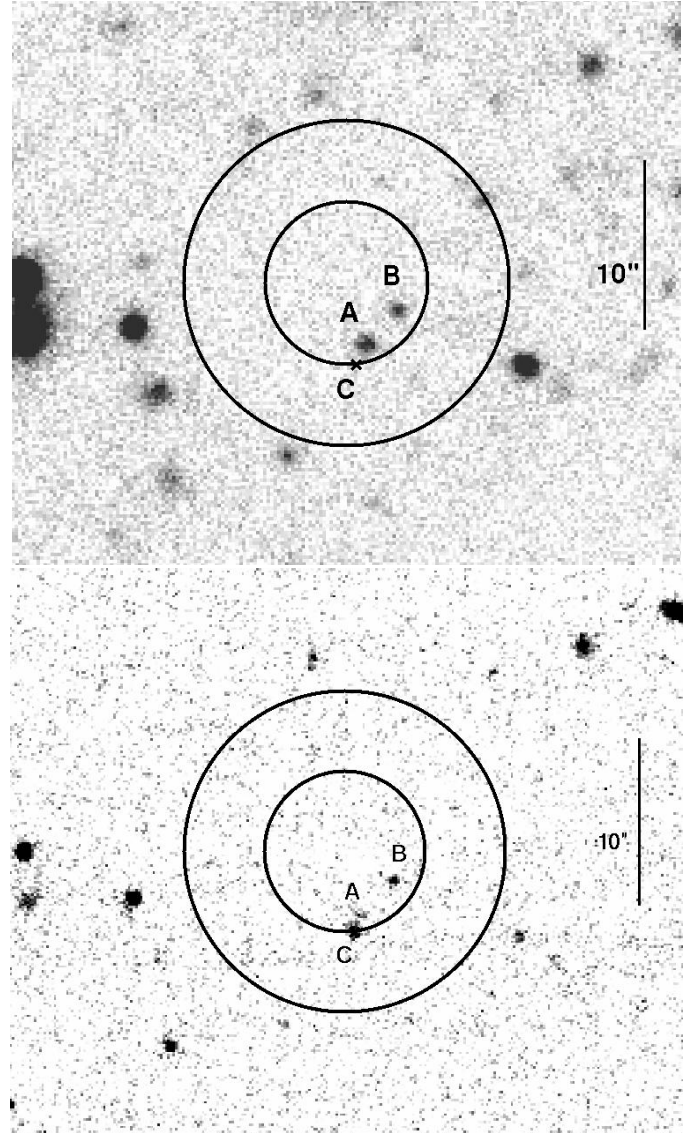

Fig. 20. VIMOS R_C-band image (*top*) and ISAAC K_s-band image (*bottom*) of the field of GRB 081105. Also shown is the 90% c.l. XRT error circle ($r_0 = 4''8$), as well as a circle of radius $2r_0$. Object C is an ERO.

reddening is very small, at $E(B - V) = 0.03$ mag. The 90% c.l. XRT error circle has $r_0 = 4''8$.

We observed the field with VIMOS and ISAAC about one year after the burst. In spite of the relatively large size of the XRT error circle, in the deep VIMOS R_C-band image we detect only two objects A and B, with AB magnitudes 23.73 ± 0.08 and 24.34 ± 0.13, respectively (Fig. 20). Both objects are also visible in the deep ISAAC K_s-band image, with AB magnitudes 22.78 ± 0.18 and 22.13 ± 0.14, respectively. In the ISAAC image, object A splits into two separate objects, with the second one (C; $K_{AB} = 21.74 \pm 0.13$) $1''0$ south of A. This object C is an ERO ($(R - K)_{AB} > 3.5$ mag). In the K_s-band image, objects A and C appear slightly extended, i.e., these might be (interacting) galaxies. In the case of B, we cannot determine whether it is a star or a galaxy.

The field was also observed by GROND while searching for the afterglow, starting about 13 h after the burst. No transient source was detected in any band; only deep upper limits could be obtained (Clemens et al. 2008; Table A.3). None of the three objects (A, B, C) were detected (Table 4).
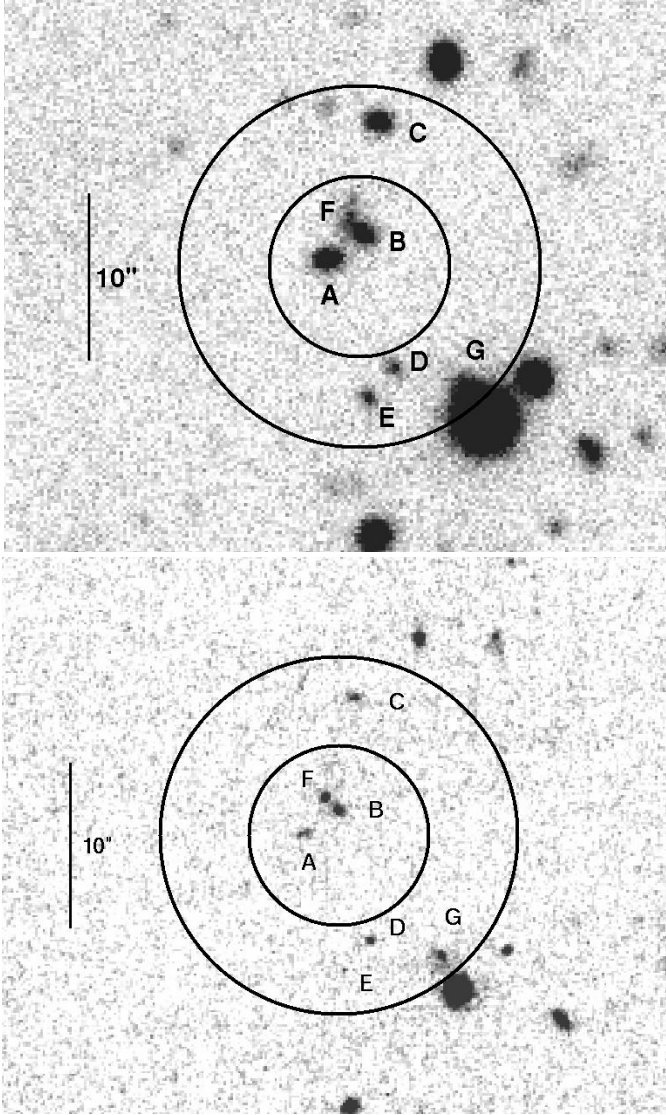
Fig. 21. VIMOS R_C-band image (*top*) and ISAAC K_s-band image (*bottom*) of the field of GRB 081204. Also shown is the 90% c.l. XRT error circle ($r_0 = 5.''3$), as well as a circle of radius $2r_0$. Object F is probably an ERO.

The $(R - K)_{AB}$ colors of objects A and B (about 0.9 mag and 2.1 mag, respectively) match those of the sample of GRBHGs at a redshift of around $z = 1$ (SBG09). The probability of finding a galaxy with the R_C-band magnitudes of objects A and B inside a field of radius $1r_0$ is $p = 0.19$ and 0.29, respectively. The probability of finding an ERO like object C inside the same field is $p_{ERO} = 0.08$. Therefore, we consider C as the most likely host galaxy candidate. We note that objects A and C could be a pair of galaxies.

GRB 081204. The field containing this object lies at moderate Galactic latitude ($b = -53°$) and is not very crowded with stars. The Galactic reddening is very small, $E(B - V) = 0.03$ mag. The 90% c.l. XRT error circle is the largest in our sample ($r_0 = 5.''3$).

We observed the field with VIMOS and ISAAC about one year after the burst. Further J-band imaging was performed with SOFI at the NTT nearly two years after the event. The field is rich in objects. Within the 90% c.l. error circle lie at least three galaxies (A, B, F; Fig. 21), which are all within $5.''0$ of each
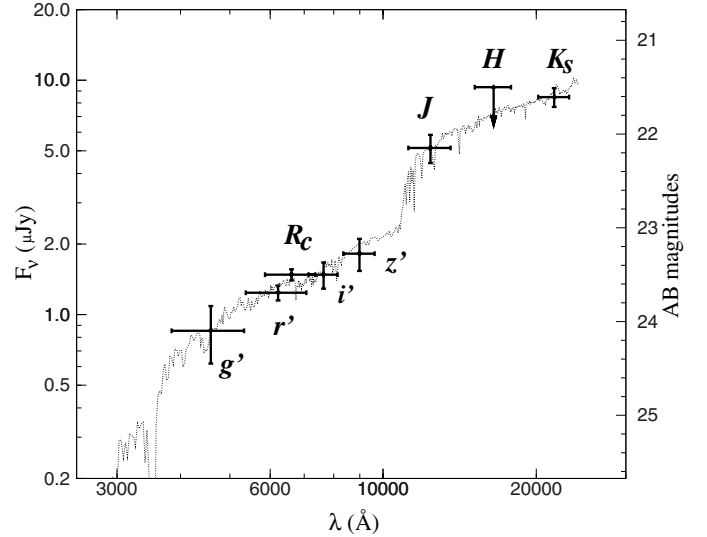

Fig. 22. *Hyperz* best-fit solution of the broad-band SED of object B in the XRT error circle of GRB 081204 (Tables 3 and 4). From left to right: GROND g', GROND r', VIMOS R_C, GROND i', GROND z', SOFI J, GROND H, and ISAAC K_s. The fit suggests that it is a spiral galaxy at a redshift of $z = 1.8 \pm 0.3$ with a moderate intrinsic SMC extinction of $A_V^{host} = 0.3$ mag (χ^2/d.o.f = 0.5).

other and could represent an interacting group. Objects A and B have similar magnitudes ($R_{AB} \sim 23.2$ and 23.5, respectively) and sizes. Object F ($R_{AB} \sim 24.6$) lies very close, northeast of object B. In the VIMOS image, it is much fainter than A and B, but in the ISAAC image it is distinctive because of its bright, point-like core ($K_{AB} = 21.5$). Within the (not so small) photometric errors, it can be classified as an extremely red object. In addition, in the VIMOS image, about $0.''7$ north of F, lies another faint, fuzzy object that is too faint for further analysis. More objects (C–E, G) are seen between $1r_0$ and $2r_0$. The brightest one is a galaxy (C) of similar magnitude and size to objects A and B. Objects D and E ($R_{AB} = 24.2$ and 24.3, respectively) have a rather blue color of $(R - K)_{AB} < 2.0$ mag and <0.0 mag, respectively. Object D is not elongated, E is only visible in the VIMOS image, while G is blended with a bright star. Given their faintness, it is difficult to establish their nature. In the ISAAC image, at least G seems to be surrounded by a faint halo, possibly indicating that this is a galaxy.

Deep follow-up observations of the field were also performed with GROND, while (unsuccessfully) searching for the afterglow about 10 h after the burst (Table A.3; Updike et al. 2008a). Objects A and B are detected in $g'r'i'z'J$, while C was only seen in $r'i'J$. Galaxy A is blue, its SED is essentially flat between R_C and K_s ($(R - K)_{AB} = 0.8 \pm 0.2$ mag), while B is redder ($(R - K)_{AB} = 1.8 \pm 0.1$ mag). Unfortunately, photometric redshift estimates are not very accurate for these galaxies.

The SED of object B shows a jump between the GROND-z' band and the SOFI-J band ($J_{AB} = 22.2$). If this is the 4000 Å Balmer break, then the redshift is 1.8 ± 0.3 (Fig. 22). Such a feature is also seen in the SED of galaxy C. We find that *Hyperz* indeed finds solutions within the redshift interval $1 < z < 2$ with different sets of extinction laws, galaxy templates, and host extinction values.

Given the connection between long GRBs and young stellar populations, it is interesting to discover an interacting group of galaxies within the 90% c.l. error circle. The magnitude-probability criterion gives for objects A and B $p = 0.16$ and

$p = 0.19$, respectively, which implies that one galaxy is not more likely than another. The probability of finding a galaxy with the red color of F within an area of radius $1r_0$ is much smaller, however, at $p_{ERO} = 0.09$. Therefore, we consider F, which is possibly interacting with B, as the most likely birthplace of GRB 081204.

4. Discussion

4.1. Magnitude-probability candidates

In the following, we call magnitude-probability candidates those galaxies that satisfy $p \leq 0.1$ (see Eq. (1), Sect. 3.2). These are: GRB 050717, objects A and B; GRB 060211A, objects A and B; GRB 060805A, objects A and B; GRB 060923B, objects A and C; GRB 070429A, objects B and C; GRB 070517, object A; GRB 080207, object B; and GRB 080602, object A. We note that in the case of GRB 070429A two galaxies have $p \leq 0.1$, and our VLT data reveal that they could constitute a tightly bound pair. We also note that the optical afterglow of GRB 070517 has been identified in the present study (Sect. 3.3) and in this case p gives the corresponding probability of finding the galaxy labeled A (Fig. 12) at the given angular distance from the afterglow position.

The other cases in our sample have $p > 0.1$, either because the detected galaxies are too faint, the XRT error circles are too big, or a mixture of both. In addition, if more than one galaxy is found inside an XRT error circle, this criterion does not tend to select one candidate over the other, as the differences in the corresponding p-values are insufficiently large (e.g., GRB 050717 and GRB 061102; Table 5). This situation changes, however, if we consider number counts of extremely red objects.

4.2. Extremely red objects as candidates

Long bursts trace the birth places of the most massive stars (e.g., Fruchter et al. 2006), which leads to the expectation that a certain percentage of hosts of long bursts are dust-enshrouded, starburst galaxies. Among them, the most extreme cases are classified as EROs. To date, only a small number of GRB hosts have been found that enter this category: GRB 020127 (Berger et al. 2007), GRB 030115 (Levan et al. 2006; Dullighan et al. 2004), GRB 080207 (Hunt et al. 2011; Svensson et al. 2012), as well as GRB 080325 (Hashimoto et al. 2010).

In our sample, seven objects fall (within their 1σ magnitude error) into this category (Table 5). These are: GRB 060923B, object D with $(R - K)_{AB} = 3.82 \pm 0.13$ mag; GRB 070429A, object D with $(R - K)_{AB} > 3.5$ mag (within the 1σ error in K_s); GRB 080207, object B with $(R - K)_{AB} = 4.66 \pm 0.40$ mag; GRB 080218B, object A with $(R - K)_{AB} = 4.15 \pm 0.16$ mag; GRB 080602, object C with $(R-K)_{AB} > 4.3$ mag; GRB 081105, object C with $(R - K)_{AB} > 3.5$ mag; and GRB 081204, object F with $(R-K)_{AB} = 3.1 \pm 0.5$ mag. Three of them lie within the corresponding 90% c.l. XRT error circle (GRB 080207, 080218B, and 081204), one object lying at $1r_0$ (GRB 081105), the other three objects lying within less than $1.5r_0$. All objects have very small p-values based on number counts of EROs on the sky (Gonzalez-Perez et al. 2009).

4.3. Lyman-dropout candidates

For two of the 17 bursts investigated here (GRBs 050922B and 080727A), we could not find any galaxy inside $2r_0$, where r_0 is the corresponding 90% c.l. XRT error circle radius. We therefore

consider the optical afterglows of these events as Lyman dropout candidates, though we cannot rule out very faint hosts at $z \lesssim 5$.

An additional, but weaker Lyman dropout candidate, is the optical afterglow of GRB 081012. Here we find only one galaxy between $1r_0$ and $2r_0$. As we have noted in Sect. 3.3, if we were to consider this as the host, then the offset of the afterglow from the center of this galaxy would be quite large. Therefore, an alternative interpretation would be that the host is not detected in our deep VLT images, i.e. it could be a Lyman drop-out.

Finally, among the seven ERO galaxies discovered in our sample, four have been detected in R, i.e. they are not Lyman drop-outs. On the other hand, these three ERO galaxies with no R-band detection could lie at higher redshifts (GRB 070429A/object D, GRB 080602/object C, and GRB 081105/object C).

We conclude that in our sample we have at best six Lyman-dropout candidates ($\sim$30%), while in all other cases this interpretation is not required[11]. This result is in qualitative agreement with other studies. Perley et al. (2009) concluded that in their uniform sample of 29 *Swift* bursts observed with the robotic Palomar 60 inch telescope, which contains 14 dark events, at most two bursts could be dark owing to a redshift $z > 4.5$. Similarly, Greiner et al. (2011) found that the fraction of high-z events among 39 dark long-duration GRBs observed with GROND in $g'r'i'z'JHK_s$ is on the order of 25%; extinction by dust in combination with a modest redshift is the main cause of the optical dimness of these events. Melandri et al. (2012) confirmed this picture using a uniform sample of 58 bright *Swift* GRBs, among which about one-third were classified as dark. They provided strong arguments that high redshift cannot be the main reason for optically dark events.

4.4. Interacting pairs of galaxies as candidates

Since long bursts are related to star formation, their host galaxies could be interacting, morphologically disturbed galaxies, where a starburst was triggered by galaxy-galaxy-interaction (e.g., Fruchter et al. 1999; Chen 2012). In our images, we find four such potential cases where at least one partner lies inside the 90% c.l. XRT error circle. These are: GRB 070429A, objects B and C (R_C band; Fig. 11); GRB 080602, objects A and C (K_s band; Fig. 15); GRB 080915A, objects C and D (R_C and K_s band; Fig. 18); as well as GRB 081204, objects B and F (R_C and K_s band; Fig. 21). In addition, object B in the field of GRB 061102 looks morphologically disturbed (Fig. 10) but no other galaxy very close to it is seen in our images.

There are no statistics at hand that could provide chance probability values for finding an interacting pair of galaxies in a randomly chosen area on the sky. Nevertheless, we conclude that the search for an interacting pair could be an effective means of finding GRB host galaxy candidates (see also Wainwright et al. 2007; Chen 2012).

4.5. Normal candidates

The fields of five bursts (GRB 050717, GRB 060211A, GRB 060805A, GRB 060919, and GRB 081012) are of particular interest in our sample. In these case, galaxy candidates

---

[11] We did not consider the two cases where a galaxy is found to be no closer than $1r_0$ from the center of the corresponding error circle (GRBs 060923B and 061102), but the galaxy's outer parts extend to within the 90% c.l. XRT error circle. In other words, here the afterglow could have been placed well inside $1r_0$.

Table 5. Summary of the properties of the objects found in the XRT error circles.

#	GRB	Object	R-band size	K_s-band size	Comment	$(R-K)_{AB}$	$(R-K)_{Vega}$	XRTpos	p	p_{ERO}
1	050717	•A	2.1 × 3.9	not visible	G	<2.08	<3.70	2	0.05 ± 0.01	
		•B	1.2 × 1.3	not visible		<2.93	<4.55	1	0.03 ± 0.01	
2	050922B	no candidates								
3	060211A	•A	1.1 × 1.2	not visible	G	<2.53	<4.16	1	0.03 ± 0.01	
		B	3.8 × 2.2	3 sources	G	1.21	2.84 ± 0.21	3	0.07 ± 0.01	
		•C	only in J	–	G	–	–	1	–	
		•D	only in J	–	–	–	–	2	–	
4	060805A	•A	1.5 × 1.1	not visible	G	<4.3	<5.9	1	0.09 ± 0.04	
		•B	2.7 × 1.3	not visible	G	<2.5	<4.1	2	0.09 ± 0.01	
5	060919	•A	1.5 × 1.4	not visible		<2.60	<4.23	1	0.15 ± 0.03	
6	060923B	•A	2.1 × 2.2	2.2 × 1.8	G	1.05	2.68 ± 0.14	2	0.06 ± 0.01	
		B	2.0 × 2.0	1.9 × 1.9	S	2.43	4.06 ± 0.04	2	–	
		•C	1.1 × 1.0	0.8 × 0.8		1.33	2.96 ± 0.16	1	0.04 ± 0.01	
		•D	1.3 × 1.3	0.8 × 0.8		3.82	5.45 ± 0.13	2	0.37 ± 0.03	0.04 ± 0.01
		•E	blended with A	blended with A				1	–	
7	061102	•A	2.5 × 1.5	not visible	G	<1.22	<2.85	2	0.34 ± 0.01	
		•B	1.8 × 1.9	not visible	G	<1.08	<2.71	2	0.31 ± 0.01	
8	**070429A**	A	3.8 × 1.4	1.9 × 1.1	G	2.10	3.73 ± 0.32	3	0.54 ± 0.05	
		•B	2.8 × 1.4	blended with C	G	1.41	3.04 ± 0.23	1	0.04 ± 0.01	
		•C	1.7 × 1.5	1.5 × 1.0	G	2.09	3.72 ± 0.16	1	0.05 ± 0.01	
		•D	not visible	1.6 × 1.0	G	>3.2	>4.8	2	–	0.07 ± 0.01
9	070517	•A	1.6 × 1.3	not visible	G	<1.69	<3.32	1	0.07 ± 0.03	
10	**080207**	A	2.4 × 1.3	not visible	G	2.08	3.71 ± 0.43	2	0.20 ± 0.02	
		•B	2.1 × 1.1	1.6 × 0.9	G	4.66	6.29 ± 0.40	1	0.14 ± 0.04	0.01 ± 0.01
11	**080218B**	•A	2.5 × 1.1	1.4 × 0.7	G	4.15	5.78 ± 0.16	1	0.12 ± 0.01	0.01
		B	1.6 × 1.5	0.8 × 0.8		1.54	3.17 ± 0.24	3	0.28 ± 0.01	
12	080602	•A	2.6 × 2.0	1.2 × 0.8	G	0.34	1.97 ± 0.05	1	0.01 ± 0.01	
		B	2.0 × 1.8	not visible	G	<0.44	<2.07	2	0.13 ± 0.01	
		•C	not visible	1.2 × 0.8	G	>4.35	>5.98	2	–	0.04 ± 0.01
13	080727A	no candidates								
14	080915A	A	3.5 × 3.5	1.2 × 1.2	S	1.11	2.74 ± 0.02	1	–	
		B	5.6 × 4.5	3.4 × 1.8	G	1.99	3.62 ± 0.01	3	0.16 ± 0.01	
		•C	1.2 × 1.2	not visible	G	<1.21	<2.83	1	0.23 ± 0.02	
		•D	1.2 × 1.2	not visible	G	<1.07	<2.69	2	0.61 ± 0.02	
		•E	1.5 × 1.5	not visible		<1.94	<3.57	1	0.37 ± 0.04	
15	081012	•A	1.8 × 1.5	not visible	G	<1.21	<2.84	2	0.31 ± 0.03	
16	081105	A	1.2 × 1.2	1.0 × 1.0	G	0.89	2.51 ± 0.20	1	0.19 ± 0.01	
		B	1.1 × 1.1	0.8 × 0.8		2.15	3.78 ± 0.19	1	0.29 ± 0.02	
		•C	not visible	0.8 × 0.5	G	>3.50	>5.13	1	–	0.08 ± 0.01
17	081204	A	2.1 × 1.4	0.9 × 0.5	G	0.78	2.40 ± 0.16	1	0.16 ± 0.01	
		B	2.7 × 1.4	1.1 × 0.8	G	1.81	3.43 ± 0.09	1	0.19 ± 0.01	
		C	2.2 × 1.7	0.9 × 0.6	G	1.04	2.66 ± 0.13	2	0.49 ± 0.02	
		D	1.2 × 1.2	0.5 × 0.5		1.97	3.59 ± 0.18	2	0.78 ± 0.03	
		E	1.2 × 1.2	not visible		<−0.04	<1.59	2	0.81 ± 0.03	
		•F	∼ 1	0.6 × 0.6	G	3.1	4.7 ± 0.50	1	0.43 ± 0.12	0.09 ± 0.01
		G	blended with a star	1.5 × 1.5		–	–	2	–	

Notes. (1) A bullet (•) in Col. #2 indicates the most likely GRB host candidate. If more than one candidate is marked then we cannot determine which is the best. For details about the selection, see Sect. 3.3. GRBs that are truly dark according to J04 and V09 are highlighted in boldface. (2) Angular sizes are given in units of arcsec. (3) Magnitude errors in $(R-K)_{AB}$ are identical to the corresponding errors for $(R-K)_{Vega}$. Colors are corrected for Galactic extinction. (4) The last two columns gives the chance probability p of finding a galaxy of the corresponding extinction-corrected (Vega) R-band magnitude on the sky in a region with the size of the corresponding X-ray error circle with a radius $r = $ XRTpos $\times r_0$ (Eq. (1)). Thereby, the first column refers to number counts of galaxies of all kinds. If the object is for sure a star, then no value is given. The second column refers to number counts of EROs only (see Sect. 4.8). (5) Comment "G" stands for galaxy, "S" for star; if no letter is given then we could not determine if this is a star or a galaxy. (6) In case of GRB 070517, the probability p is based on the distance between the afterglow and galaxy A (1″6; Sect. 3.3). GRB 070429A/object D, and GRB 081204/object F are EROs within the large 1σ photometric error (see Table 3).

are seen in the corresponding XRT error circle, at least within $2r_0$, but no EROs are found, nor is there evidence of an interacting pair. We must conclude that if one of these is the host, then it is a normal galaxy, i.e., typical of the host galaxies of non-extinguished GRBs. This agrees with Perley et al. (2009), who found that in their sample most of the hosts galaxies of dark GRBs do not differ phenomenologically from the hosts of bursts with optically detected afterglows.

A special case is GRB 070517, for which we were able to identify the optical afterglow based on the early observations by Fox et al. (2007). Here only one object is found within $1r_0$, but this object is offset from the position of the optical afterglow by $1''6$. If this is the host then a redshift $z \lesssim 0.5$ is required in order to avoid a projected offset in kpc which is rather large compared to the observed mean of the GRB offset distribution (Bloom et al. 2002). This redshift then provides further evidence of a subluminous galaxy (see Sect. 4.6), although no strong constraints on its properties can be obtained.

4.6. Redshift estimates

No precise redshifts are known for the galaxies we have found in the XRT error circles; only rough estimates can be obtained. A first approach is the estimation of the photometric redshift by SED fitting using *Hyperz*. We decided to apply this method only to the objects inside a XRT error circle that are considered to be the GRB host candidates. Since this approach requires a well-sampled optical/NIR SED (Tables 4 and 5), it was possible to use it in only two cases. For GRB 080602/object A we obtain $z = 1.40^{+0.30}_{-0.15}$ (Fig. 16). One could then speculate that this is also the redshift of the ERO just $1''3$ north of A (object C; Fig. 15). For GRB 081204/object B, we find $z = 1.8 \pm 0.3$ (Fig. 22). One can then again speculate that this is also the redshift of the ERO about $1''$ northeast of it (object F; Fig. 21).

A second approach for estimating z is more statistical. In Table A.2, we provide estimated redshifts by assuming that the galaxies have absolute magnitudes of $M_R = -22, -20$, and -18, respectively. The first value is about 1 mag below the most luminous galaxies found in the Las Campanas redshift survey ($M_R = -23$; Lin et al. 1996). The middle value is approximately the characteristic $M^\star$ of the corresponding Schechter r-band luminosity function. The third value roughly corresponds to the absolute magnitude of the Large Magellanic Cloud. By adopting a power-law spectrum for the SED of the form $F_\nu \propto \nu^{-\beta}$, we then calculated the corresponding redshift for two different spectral slopes ($\beta = 0.0$ and 1.0)[12]. We find that most galaxies would lie at redshifts $z < 2$ if their luminosity were lower than that of the Milky Way.

Finally, we used the $E_{\rm peak}$-$E_{\rm iso}$ correlation for long GRBs (Amati 2006) by analyzing the *Swift*/BAT or *Konus-WIND* spectrum. Unfortunately, for the majority of the bursts the required spectral information for this analysis is not available. Only in five cases did we obtain results, though they are not tight constraints (Table A.1). In the case of GRB 080207 and GRB 080602, the $E_{\rm peak} - E_{\rm iso}$ relation constrains the redshift to be $z > 0.9$ (2σ) and $z > 1$ (2σ), respectively, in agreement with the redshifts found for GRB 080207 ($z \sim 2.2$; Hunt et al. 2011, and Sect. 3.3) and GRB 080602 ($z \sim 1.4$; Sect. 3.3).

4.7. Host galaxy candidates of truly dark bursts

Fynbo et al. (2009) shows that at least 39% of optically dim GRB afterglows are dark according to the J04 criterion. In our sample, GRB 070429A, GRB 080207, and GRB 080218B are truly optically dark (Sect. 2.3) and also belong to our small subsample of bursts with extremely red host galaxy candidates (Sect. 4.2). This supports the idea that global dust extinction in their host galaxies was responsible for dimming the afterglow in the optical bands. This holds especially for GRB 080207, for which we can be sure that the host galaxy is object B, thanks to the precise localization of its X-ray afterglow by *Chandra*.

In the case of GRB 080218B, the host galaxy candidate is visible in the $R_{\rm C}$-band, constraining its redshift to be $\lesssim 5$. For this event, Greiner et al. (2011) found that different pairs of (z, A_V) solutions can explain the non-detection of the optical/NIR afterglow by GROND. For example, for a redshift of 3.5 a host extinction of $A_V^{\rm host} = 1.5$ mag is required. A lower redshift would increase the deduced amount of host extinction even more; however, studies of *optically detected* afterglows (e.g., Kann et al. 2010) show that these extinction values would be very high compared to the average. Nevertheless, host galaxies with low extinction may be linked to the optical detection of GRB afterglows; more statistics are needed to establish how common high values of extinction really are.

Another ERO, the host candidate D of GRB 070429A that was not detected in $R_{\rm C}$, lies just on the border of the 90% c.l. XRT error circle. It is a less compelling host candidate because it is also very faint in $K_{\rm s}$, with a correspondingly large photometric error of 0.4 mag. In this case, there are also two more galaxies within the 90% c.l. error circle. Their $(R-K)$, however, colors are notparticularly red. If the very red galaxy were to be confirmed as an ERO, then our study would indicate that there is a strong link between optically dark GRBs and ERO galaxies.

4.8. EROs as an important subpopulation of GRB host galaxies

The seven EROs that we have identified have magnitudes between $K_{\rm AB} = 21.5$ and 23.0, i.e. $K_{\rm Vega} = 19.6$ to 21.1 (Table 3). For these K-band magnitudes, the number density of EROs on the sky is on the order of 1 per 1000 arcsec^2 (Gonzalez-Perez et al. 2009; Hempel et al. 2011; Kim et al. 2011)[13]. Our findings then imply that there is an overdensity of EROs in the XRT error circles that we have studied here. Four of the seven EROs that we have found lie inside their corresponding 90% c.l. XRT error circle. In the remaining three cases (GRBs 060923B, 070429A, and 080602), the ERO lies just close to the border of the 90% c.l. error circle.

Since long GRBs are thought to trace the formation of massive stars (passively evolving ellipticals cannot be their hosts), the results obtained with our study suggest that bursts with optically non-detected afterglows (but with rapid and deep follow-up observations) trace a subpopulation of massive galaxies undergoing violent star formation. This holds for dark bursts in particular: all three bursts investigated here that belong to this class have an ERO within or close to their 90% c.l. XRT error circle (GRB 070429A, GRB 080207, and GRB 080218B). If we consider as dark all GRBs that follow the J04 *or* V09 criterion (but keeping in mind that this now includes events where the X-ray data are not so easily interpreted, see Sect. 2.3), then we have

---

[12] Thereby, the absolute R-band magnitude is given by $M_R = m_R - \mu - k$, where μ is the distance modulus and k is the cosmological k-correction, $k = -2.5 (1 - \beta) \log(1 + z)$. If the deduced redshift is higher than 5, the Lyman dropout in the R-band could have affected the apparent magnitudes and no values for z are given.

[13] More precisely, we used Fig. 10 in Gonzalez-Perez et al. (2009) to calculate chance probability values for EROs (Table 5).

eight of these GRBs in our sample (Table 2); five of them have an ERO within or close to their 90% c.l. error circle (in addition GRBs 080602 and 081204). It should be stressed that, in principle, all GRBs studied here except GRB 070517 (for which we identified the afterglow; Sect. 3.3) could be truly dark bursts according to the criterion from J04 and V09; we just do not have sufficiently deep optical limits to be certain.

Several previous studies have targeted GRBHs (e.g., Le Floc'h et al. 2003; Christensen et al. 2004; Fruchter et al. 2006; Ovaldsen et al. 2007; Svensson et al. 2010; Levesque et al. 2010; and SBG09). They have focused on the low-redshift regime (up to $z \sim 1.5$) and showed that most hosts are subluminous ($L < L^*$), blue, of low metallicity and with a moderate star formation rate ($\sim 1-10\ M_\odot\ \mathrm{yr}^{-1}$). However, our results suggest that an infrared-bright subpopulation of very dusty GRBHs exists, which stands out from the main GRB host galaxy population.

Redshift measurements for the EROs that we have identified here are missing in most cases. However, for the ERO related to GRB 080207, a photometric redshift was derived by Hunt et al. (2011). The observed broad-band SED is indicative of a very luminous ($M_K \sim 24.4$), infrared-bright galaxy, very different from the sample of GRBHs compiled by SBG09. This host galaxy is similar in color, luminosity, and redshift to the hosts of the dark bursts GRB 020127 (Berger et al. 2007), GRB 030115 (Levan et al. 2006), and GRB 080325 (Hashimoto et al. 2010). There is possibly a bias in the GRB host samples studied so far, which are dominated by host galaxies of optically detected afterglows. This conclusion is supported by recent work on dark bursts observed with GROND (Krühler et al. 2011), where it is shown that highly extinguished afterglows trace a subpopulation of luminous, massive, metal-rich, and chemically evolved GRBHs that were not previously associated with GRBs.

5. Summary

Motivated by the non-detection of the optical afterglows of a substantial fraction of *Swift* bursts with well-observed X-ray afterglows, we have selected 17 of these events with small *Swift*/XRT error circles (defined by their individual 90% c.l. radius r_0) and searched for the potential host galaxies of these bursts using deep multi-color imaging. Our primary telescope was the VLT equipped with FORS1, FORS2, and VIMOS for R_C-band imaging and ISAAC and HAWK-I for K_s-band imaging. These data were supplemented by observations with the seven-channel imager GROND mounted at the 2.2-m MPG/ESO telescope on La Silla and the infrared imager NEWFIRM mounted at the 4-m Mayall telescope on Kitt Peak. The limiting magnitudes we achieved are deep, at usually $R_{AB} = 26.5$ and $K_{AB} = 23.5$ as well as $g'r'i'z'JHK = 25.5, 25, 24.5, 24, 22.5, 21.5,$ and 21 for GROND. The latter data include late-time imaging as well as data gained in rapid response mode, where we did not find evidence of a fading afterglow.

We have discovered up to six events, about one-third of our sample, where the corresponding GRB host galaxy could be Lyman dropped out in the R_C band. In two cases, we do not see any object within an area of twice the radius of each associated 90% c.l. *Swift*/XRT error circle down to deep flux limits (GRBs 050922B and 080727A); in one event, there is only one galaxy within $1r_0$ and $2r_0$ (GRB 081012); and three bursts have a very red galaxy detected only in the K_s-band (GRB 070429A/object D, GRB 080602/object C, GRB 081105/object C). These three bursts belong to a subsample of seven bursts for which we found that an ERO, which we

recall are defined as having $(R - K)_{AB} > 3.5$ mag, was the confirmed or likely host galaxy. In particular, all three bursts in our sample that are classified as securely dark according to their observed X-ray flux (following J04 and V09) belong to this group. Even though these are small number statistics, our findings imply that a non-negligible fraction of optically dim bursts may be located in globally dust-enshrouded galaxies.

While the $(R - K)$ color of galaxies has emerged as a powerful criterion for identifying host galaxy candidates, we also considered chance-probability constraints based on published number counts of (all types of) galaxies on the sky. In nine bursts, the chance probability p of finding a galaxy of the given R_C-band magnitude in the corresponding 90% c.l. XRT error circle is $\leq 10\%$ (within 1σ), which makes them good host galaxy candidates. In the remaining cases (about 1/2 of our sample), galaxies were identified but they are not special in any way, in terms of either their $(R - K)$ colors, their magnitudes, or their p-values. However, for four bursts, we have discovered possibly interacting galaxies in the XRT error circle, which is potentially a sign of triggered star-formation.

The connection between star-forming activity and dark bursts is even more intriguing for the seven EROs in our sample. This is the most outstanding result of our study. It points to the existence of a subpopulation of GRBHs, characterized by violent star formation, that is missed by host galaxy surveys of bursts with detected optical afterglows. The putative host of GRB 080207 is the most remarkable example ($(R - K)_{AB} = 4.66 \pm 0.40$ mag; Hunt et al. 2011; Svensson et al. 2012). The possibility that a non-negligible fraction of optically dim bursts are highly dust-enshrouded and possibly submm-bright galaxies makes these bursts interesting cosmological tools for achieving a deeper insight into the optically obscured star-formation history of the Universe (Berger et al. 2003; Tanvir et al. 2004).

References

Amati, L. 2006, MNRAS, 372, 233
Andreev, M., Kurenya, A., & Pozanenko, A. 2008, GCN Circ., 7333
Appenzeller, I., Fricke, K., Fürtig, W., et al. 1998, The Messenger, 94, 1

Autry, R. G., Probst, R. G., Starr, B. M., et al. 2003, in SPIE Conf. Ser. 4841, eds. M. Iye, & A. F. M. Moorwood, 525

Barbier, L., Barthelmy, S., Cummings, J., et al. 2006a, GCN Circ., 5403

Barbier, L., Barthelmy, S. D., Cummings, J., et al. 2006b, GCN Circ., 5595

Barthelmy, S. D., Barbier, L. M., Cummings, J. R., et al. 2005, Space Sci. Rev., 120, 143

Barthelmy, S. D., Markwardt, C. B., Page, K. L., et al. 2007, GCN Circ., 6355

Beardmore, A. P., & Cummings, J. 2008, GCN Circ., 8487

Beardmore, A. P., Barthelmy, S. D., Cummings, J. R., et al. 2008a, GCN Circ., 7781

Beardmore, A. P., Burrows, D. N., & Cummings, J. R. 2008b, GCN Circ., 8522

Beardmore, A. P., Evans, P. A., Goad, M. R., & Osborne, J. P. 2008c, GCN Circ., 7782

Beardmore, A. P., Page, K. L., & Evans, P. A. 2008d, GCN Circ., 7785

Beardmore, A. P., Page, K. L., Evans, P. A., et al. 2008e, GCN Rep., 145

Berger, E., & Lopez-Morales, M. 2005, GCN Circ., 3639

Berger, E., & Rest, A. 2008, Circ, 8624

Berger, E., Cowie, L. L., Kulkarni, S. R., et al. 2003, ApJ, 588, 99

Berger, E., Lopez-Morales, M., & Osip, D. 2005, GCN Circ., 3643

Berger, E., Fox, D. B., Kulkarni, S. R., Frail, D. A., & Djorgovski, S. G. 2007, ApJ, 660, 504

Bissaldi, E. 2008, GCN Circ., 8370

Bloom, J. S., Kulkarni, S. R., & Djorgovski, S. G. 2002, AJ, 123, 1111

Blustin, A., Hurkett, C., Smale, A., & Cominsky, L. 2005, GCN Circ., 3638

Bolzonella, M., Miralles, J.-M., & Pelló, R. 2000, A&A, 363, 476

Breeveld, A., & Guidorzi, C. 2006, GCN Circ., 5580

Breeveld, A., & Oates, S. R. 2008, GCN Circ., 8232

Burrows, D. N., Hill, J. E., Nousek, J. A., et al. 2005, Space Sci. Rev., 120, 165

Butler, N. R. 2007, AJ, 133, 1027

Cannizzo, J., Barbier, L., Barthelmy, S. D., et al. 2007, GCN Circ., 6362

Castro-Tirado, A. J., Cunniffe, R., de Ugarte Postigo, A., et al. 2006, in SPIE Conf. Ser., 6267

Castro-Tirado, A. J., Bremer, M., McBreen, S., et al. 2007, A&A, 475, 101

Cenko, S. B. 2006, GCN Circ., 5401

Cenko, S. B., Kelemen, J., Harrison, F. A., et al. 2009, ApJ, 693, 1484

Chen, H.-W. 2012, MNRAS, 419, 3039

Christensen, L., Hjorth, J., & Gorosabel, J. 2004, A&A, 425, 913

Clemens, C., Filgas, R., Greiner, J., et al. 2008, GCN Circ., 8492

Cobb, B. E. 2008a, GCN Circ., 7318

Cobb, B. E. 2008b, GCN Circ., 8248

Conselice, C. J., Bundy, K., U, V., et al. 2008, MNRAS, 383, 1366

Covino, S., D'Avanzo, P., Antonelli, L. A., et al. 2008a, GCN Circ., 7322

Covino, S., D'Avanzo, P., Antonelli, L. A., et al. 2008b, GCN Circ., 8233

Cucchiara, A., & Fox, D. B. 2008, GCN Circ., 7276

Cucchiara, A., & Racusin, J. 2008, GCN Circ., 7268

Cucchiara, A., Levan, A. J., Fox, D. B., et al. 2011, ApJ, 736, 7

Cummings, J., Barbier, L., Barthelmy, S., et al. 2005a, GCN Circ., 3637

Cummings, J., Barbier, L., Barthelmy, S., et al. 2005b, GCN Circ., 4033

Cummings, J., Barthelmy, S., Gehrels, N., et al. 2008, GCN Circ., 8484

Curran, P. A., Schady, P., & Cummings, J. 2008, GCN Circ., 8488

D'Avanzo, P., Antonelli, L. A., Covino, S., et al. 2008, GCN Circ., 7269

De Pasquale, M., Piro, L., Perna, R., et al. 2003, ApJ, 592, 1018

de Ugarte Postigo, A., & Malesani, D. 2008, GCN Circ., 8366

de Ugarte Postigo, A., Castro-Tirado, A. J., Jelinek, M., et al. 2007, GCN Circ., 6361

Doherty, M., Bunker, A. J., Ellis, R. S., & McCarthy, P. J. 2005, MNRAS, 361, 525

Dullighan, A., Ricker, G., Butler, N., & Vanderspek, R. 2004, in Gamma-Ray Bursts: 30 Years of Discovery, eds. E. Fenimore, & M. Galassi, AIP Conf. Ser., 727, 467

Elston, R., Rieke, G. H., & Rieke, M. J. 1988, ApJ, 331, L77

Evans, P. A. 2011a, GCN, 12250

Evans, P. A. 2011b, GCN, 12273

Evans, P. A., & Oates, S. R. 2008, GCN Circ., 8231

Evans, P. A., Beardmore, A. P., Page, K. L., et al. 2007, A&A, 469, 379

Evans, P. A., Goad, M. R., Osborne, J. P., & Beardmore, A. P. 2008, GCN Circ., 8391

Evans, P. A., Beardmore, A. P., Page, K. L., et al. 2009, MNRAS, 397, 1177

Evans, I. N., Primini, F. A., Glotfelty, K. J., et al. 2010, ApJS, 189, 37

Filgas, R., Kruehler, T., Greiner, J., et al. 2008, GCN Circ., 8373

Fontanot, F., & Monaco, P. 2010, MNRAS, 405, 705

Fox, D. B., Price, P. A., & Berger, E. 2007, GCN Circ., 6420

French, J., Jelinek, M., Kubanek, P., & de Ugarte Postigo, A. 2008, GCN Circ., 7316

Fruchter, A. S., Thorsett, S. E., Metzger, M. R., et al. 1999, ApJ, 519, L13

Fruchter, A. S., Levan, A. J., Strolger, L., et al. 2006, Nature, 441, 463

Fugazza, D., D'Elia, V., D'Avanzo, P., Covino, S., & Tagliaferri, G. 2008, GCN Circ., 7293

Fynbo, J. U., Jensen, B. L., Gorosabel, J., et al. 2001, A&A, 369, 373

Fynbo, J. P. U., Jakobsson, P., Prochaska, J. X., et al. 2009, ApJS, 185, 526

Gehrels, N., Chincarini, G., Giommi, P., et al. 2004, ApJ, 611, 1005

Gilmore, A. C. 2007, GCN Circ., 6412

Godet, O., Page, K. L., Osborne, J. P., et al. 2005, GCN Circ., 4031

Golenetskii, S., Aptekar, R., Mazets, E., et al. 2005, GCN Circ., 3640

Golenetskii, S., Aptekar, R., Mazets, E., et al. 2008, GCN Circ., 7784

Gomboc, A., Guidorzi, C., Steele, I. A., et al. 2006, GCN Circ., 4738

Gonzalez-Perez, V., Baugh, C. M., Lacey, C. G., & Almeida, C. 2009, MNRAS, 398, 497

Gonzalez-Perez, V., Baugh, C. M., Lacey, C. G., & Kim, J.-W. 2011, MNRAS, 417, 517

Gorosabel, J., Christensen, L., Hjorth, J., et al. 2003, A&A, 400, 127

Götz, D., Mereghetti, S., Paizis, A., et al. 2008, GCN Circ., 8614

Greiner, J., Bornemann, W., Clemens, C., et al. 2008, PASP, 120, 405

Greiner, J., Krühler, T., Fynbo, J. P. U., et al. 2009, ApJ, 693, 1610

Greiner, J., Krühler, T., Klose, S., et al. 2011, A&A, 526, A30

Guidorzi, C., Barthelmy, S. D., Evans, P. A., et al. 2006a, GCN Circ., 5575

Guidorzi, C., Romano, P., Moretti, A., & Vergani, S. 2006b, GCN Circ., 5577

Guziy, S., Jelinek, M., Gorosabel, J., et al. 2005, GCN Circ., 4025

Haislip, J. B., Nysewander, M. C., Reichart, D. E., et al. 2006, Nature, 440, 181

Hashimoto, T., Ohta, K., Aoki, K., et al. 2010, ApJ, 719, 378

Hempel, A., Cristóbal-Hornillos, D., Prieto, M., et al. 2011, MNRAS, 414, 2246

Hogg, D. W., Pahre, M. A., McCarthy, J. K., et al. 1997, MNRAS, 288, 404

Holland, S. T. 2006, GCN Circ., 5784

Holland, S., & Cucchiara, A. 2006, GCN Circ., 5603

Holland, S. T., Barthelmy, S. D., Chester, M. M., et al. 2006, GCN Circ., 5776

Holland, S. T., Sbarufatti, B., Shen, R., et al. 2010, ApJ, 717, 223

Hunt, L., Palazzi, E., Rossi, A., et al. 2011, ApJ, 736, L36

Hurkett, C., Page, K., Burrows, D., et al. 2005a, GCN Circ., 3636

Hurkett, C., Page, K., Kennea, J., et al. 2005b, GCN Circ., 3633

Hurkett, C., Beardmore, A., Godet, O., et al. 2006, GCN Circ., 4736

Immler, S., Baumgartner, W. H., Gehrels, N., et al. 2008, GCN Circ., 8021

Jakobsson, P., Hjorth, J., Fynbo, J. P. U., et al. 2004, ApJ, 617, L21 (J04)

Kann, D. A., Klose, S., Zhang, B., et al. 2010, ApJ, 720, 1513

Kann, D. A., Klose, S., Zhang, B., et al. 2011, ApJ, 734, 96

Kawai, N., Kosugi, G., Aoki, K., et al. 2006, Nature, 440, 184

Kennea, J. A., & Stroh, M. 2008, GCN Circ., 8364

Kennea, J. A., Burrows, D. N., Hurkett, C., Page, K., & Gehrels, N. 2005, GCN Circ., 3634

Khamitov, I., Kose, O., Yakut, K., et al. 2008, GCN Circ., 7270

Kim, J.-W., Edge, A. C., Wake, D. A., & Stott, J. P. 2011, MNRAS, 410, 241

Kissler-Patig, M., Pirard, J.-F., Casali, M., et al. 2008, A&A, 491, 941

Klose, S., Eislöffel, J., & Richter, S. 1996, ApJ, 470, L93

Klose, S., Greiner, J., Rau, A., et al. 2004, AJ, 128, 1942

Klotz, A., Boer, M., & Atteia, J. L. 2006, GCN Circ., 5576

Klotz, A., Boer, M., & Atteia, J. L. 2008, GCN Circ., 7267

Kong, X., Fang, G., Arimoto, N., & Wang, M. 2009, ApJ, 702, 1458

Kornienko, G., Rumyantsev, V., & Pozanenko, A. 2005, GCN Circ., 4047

Kouveliotou, C., Meegan, C. A., Fishman, G. J., et al. 1993, ApJ, 413, L101

Krimm, H., Barbier, L., Barthelmy, S., et al. 2006a, GCN Circ., 4757

Krimm, H. A., Hurkett, C., Pal'shin, V., et al. 2006b, ApJ, 648, 1117

Krühler, T., Küpcü Yoldaş, A., Greiner, J., et al. 2008, ApJ, 685, 376

Krühler, T., Greiner, J., Schady, P., et al. 2011, A&A, 534, A108

Krühler, T., Malesani, D., Milvang-Jensen, B., et al. 2012, ApJ, submitted [arXiv:1205.4036]

Kuin, N. P. M., & Stroh, M. C. 2008, GCN Circ., 8365

Küpcü Yoldaş, A., Yoldaş, A., Greiner, J., et al. 2008, GCN Circ., 7279

Küpcü Yoldaş, A., Greiner, J., Klose, S., Krühler, T., & Savaglio, S. 2010, A&A, 515, L2

Landsman, W. B., & Immler, S. 2008, GCN Circ., 8027

Le Fèvre, O., Saisse, M., Mancini, D., et al. 2003, in SPIE Conf. Ser. 4841, eds. M. Iye, & A. F. M. Moorwood, 1670

Le Floc'h, E., Duc, P., Mirabel, I. F., et al. 2003, A&A, 400, 499

Levan, A. J., & Wiersema, K. 2008, GCN Circ., 8048

Levan, A., Fruchter, A., Rhoads, J., et al. 2006, ApJ, 647, 471

Levesque, E. M., Berger, E., Kewley, L. J., & Bagley, M. M. 2010, AJ, 139, 694

Li, W. 2006, GCN Circ., 5400

Lin, H., Kirshner, R. P., Shectman, S. A., et al. 1996, ApJ, 464, 60

Lipunov, V., Kornilov, V., Kuvshinov, D., et al. 2006, GCN Circ., 4741

Luckas, P., Trondal, O., & Schwartz, M. 2005, GCN Circ., 3642

MacLeod, C., Kirschbrown, J., Haislip, J., et al. 2005, GCN Circ., 3652

Malesani, D., Jakobsson, P., Levan, A. J., Rol, E., & Fynbo, J. P. U. 2008a, GCN Circ., 8039

Malesani, D., Quirion, P., Fynbo, J. P. U., & Jakobsson, P. 2008b, GCN Circ., 7783

Malesani, D., Quirion, P., Fynbo, J. P. U., & Jakobsson, P. 2008c, GCN Circ., 7783

Mangano, V., Sbarufatti, B., La Parola, V., & Baumgartner, W. H. 2008a, GCN Circ., 8620

Mangano, V., Sbarufatti, B., & Parola, V. L. 2008b, GCN Circ., 8616

Marìn, V. M., Sabater, J., Castro-Tirado, A. J., et al. 2008, GCN Circ., 7291

McLean, K., Barthelmy, S. D., Baumgartner, W., et al. 2008, GCN Circ., 8029

Melandri, A., Gomboc, A., Smith, R. J., & Tanvir, N. 2006, GCN Circ., 5579

Melandri, A., Sbarufatti, B., D'Avanzo, P., et al. 2012, MNRAS, 421, 1265

Moin, A., Tingay, S., Phillips, C., et al. 2008, GCN Circ., 8466

Moorwood, A., Cuby, J.-G., Biereichel, P., et al. 1998a, The Messenger, 94, 7

Moorwood, A., Cuby, J.-G., & Lidman, C. 1998b, The Messenger, 91, 9

Muehlegger, M., Duscha, S., Stefanescu, A., et al. 2006, GCN Circ., 5405

Norris, J., Barbier, L., Barthelmy, S., et al. 2005, GCN Circ., 4008

Norris, J., Kutyrev, A., Ganguly, R., Canterna, R., & Pierce, M. 2006, GCN Circ., 4760

Oates, S. R., Beardmore, A. P., Cummings, J. R., et al. 2008a, GCN Circ., 8227

Oates, S. R., Ukwatta, T. N., Evans, P., & Breeveld, A. 2008b, GCN Rep., 168, 1

Ovaldsen, J.-E., Jaunsen, A. O., Fynbo, J. P. U., et al. 2007, ApJ, 662, 294

Pandey, S. B., Page, M. J., Ziaeepour, H. Z., & Oates, S. R. 2006, GCN Circ., 5402

Pasquale, M. D., Norris, J., Kennedy, T., Mason, K., & Gehrels, N. 2005, GCN Circ., 4028

Pérez-Ramírez, D., de Ugarte Postigo, A., Gorosabel, J., et al. 2010, A&A, 510, A105

Perley, D. A., Cenko, S. B., Bloom, J. S., et al. 2009, AJ, 138, 1690

Piro, L., Frail, D. A., Gorosabel, J., et al. 2002, ApJ, 577, 680

Price, P. A. 2007, GCN Circ., 6371

Racusin, J. L., Barthelmy, S. D., Baumgartner, W. H., et al. 2008, GCN Circ., 7264

Rieke, G. H., & Lebofsky, M. J. 1985, ApJ, 288, 618

Rol, E., & Page, K. L. 2006, GCN Circ., 5406

Rol, E., Wijers, R. A. M. J., Kouveliotou, C., Kaper, L., & Kaneko, Y. 2005, ApJ, 624, 868

Rol, E., van der Horst, A., Wiersema, K., et al. 2007, ApJ, 669, 1098

Roming, P. W. A., Kennedy, T. E., Mason, K. O., et al. 2005, Space Sci. Rev., 120, 95

Rossi, A., de Ugarte Postigo, A., Ferrero, P., et al. 2008a, A&A, 491, L29

Rossi, A., Greiner, J., Küpcü Yoldaş, A., & Yoldaş, A. 2008b, GCN Circ., 7319

Rossi, A., Kruehler, T., Greiner, J., et al. 2008c, GCN Circ., 8268

Rossi, A., Schulze, S., Klose, S., et al. 2011, A&A, 529, A142

Rujopakarn, W., Rykoff, E. S., Schaefer, B. E., Yuan, F., & Yost, S. A. 2006, GCN Circ., 4737

Rujopakarn, W., Swan, H., & Guver, T. 2008, GCN Circ., 8228

Rykoff, E. S., Schaefer, B. E., & Swan, H. 2007, GCN Circ., 6356

Salvaterra, R., Della Valle, M., Campana, S., et al. 2009, Nature, 461, 1258

Sari, R., Piran, T., & Narayan, R. 1998, ApJ, 497, L17

Sato, G., Barbier, L., Barthelmy, S., et al. 2006a, GCN Circ., 4751

Sato, G., Barbier, L., Barthelmy, S. D., et al. 2006b, GCN Circ., 5578

Savaglio, S., Glazebrook, K., & Le Borgne, D. 2009, ApJ, 691, 182 (SBG09)

Schady, P., & Cannizzo, J. 2007, GCN Circ., 6364

Schady, P., Barthelmy, S. D., Baumgartner, W. H., et al. 2008a, GCN Circ., 7314

Schady, P., Evans, P. A., & Krimm, H. 2008b, GCN Rep., 117

Schaefer, B. E., Cline, T. L., Hurley, K. C., & Laros, J. G. 1998, ApJS, 118, 353

Schaefer, B. E., Quimby, R., Yost, S. A., & Rujopakarn, W. 2005, GCN Circ., 4010

Schlegel, D. J., Finkbeiner, D. P., & Davis, M. 1998, ApJ, 500, 525

Sharapov, D., Ibrahimov, M., Pozanenko, A., & Rumyantsev, V. 2006, GCN Circ., 4927

Sonoda, E., Maeno, S., Tokunaga, Y., & Yamauchi, M. 2005, GCN Circ., 4009

Spergel, D. N., Verde, L., Peiris, H. V., et al. 2003, ApJS, 148, 175

Stamatikos, M., Barthelmy, S. D., Burrows, D. N., et al. 2006, GCN Circ., 5590

Stamatikos, M., Barthelmy, S. D., Cummings, J., et al. 2008, GCN Circ., 7277

Starling, R. L. C., Page, K. L., & Holland, S. T. 2006, GCN Circ., 5783

Svensson, K. M., Levan, A. J., Tanvir, N. R., Fruchter, A. S., & Strolger, L. 2010, MNRAS, 405, 57

Svensson, K. M., Tanvir, N. R., Perley, D. A., et al. 2012, MNRAS, 421, 25

Tagliaferri, G., Antonelli, L. A., Chincarini, G., et al. 2005, A&A, 443, L1

Tanvir, N. R., Barnard, V. E., Blain, A. W., et al. 2004, MNRAS, 352, 1073

Tanvir, N. R., Fox, D. B., Levan, A. J., et al. 2009, Nature, 461, 1254

Tody, D. 1993, in Astronomical Data Analysis Software and Systems II, eds. R. J. Hanisch, R. J. V. Brissenden, & J. Barnes, ASP Conf. Ser., 52, 173

Torii, K. 2005, GCN Circ., 4024

Tueller, J., Barbier, L., Barthelmy, S. D., et al. 2006, GCN Circ., 5777

Ukwatta, T., Barthelmy, S. D., Baumgartner, W., et al. 2008, GCN Circ., 8230

Updike, A., Clemens, C., & Greiner, J. 2008a, GCN Circ., 8627

Updike, A. C., Milne, P. A., Williams, G. G., & Hartmann, D. H. 2008b, GCN Circ., 7273

Urata, Y., Kuwahara, M., Tashiro, M., et al. 2006, GCN Circ., 5204

van der Horst, A. J., Kouveliotou, C., Gehrels, N., et al. 2009, ApJ, 699, 1087 (V09)

Vergani, S. D., Barthelmy, S. D., Beardmore, A. P., et al. 2007a, GCN Circ., 6411

Vergani, S. D., Romano, P., Guidorzi, C., et al. 2007b, GCN Rep., 56.2

Vrba, F. J., Hartmann, D. H., & Jennings, M. C. 1995, ApJ, 446, 115

Vrba, F. J., Luginbuhl, C. B., Jennings, M. C., & Hartmann, D. H. 1999, ApJ, 511, 298

Vreeswijk, P., Fynbo, J., Milvang-Jensen, B., et al. 2008, GCN Circ., 7327

Wainwright, C., Berger, E., & Penprase, B. E. 2007, ApJ, 657, 367

Yoldaş, A. K., Krühler, T., Greiner, J., et al. 2008, in AIP Conf. Ser. 1000, eds. M. Galassi, D. Palmer, & E. Fenimore, 227

Ziaeepour, H. Z., Barthelmy, S. D., Cummings, J. R., et al. 2006, GCN Circ., 5398

[1] Thüringer Landessternwarte Tautenburg, Sternwarte 5, 07778 Tautenburg, Germany
e-mail: rossi@tls-tautenburg.de

[2] Instituto de Astrofísica de Canarias (IAC), 38200 La Laguna, Tenerife, Spain

[3] Departamento de Astrofísica, Universidad de La Laguna (ULL), 38205 La Laguna, Tenerife, Spain

[4] Max-Planck-Institut für Extraterrestrische Physik, Giessenbachstraße, 85748 Garching, Germany

[5] University of Rochester, Department of Physics and Astronomy, Rochester, NY 14627-0171, USA

[6] Florida Institute of Technology, Melbourne, FL 32901, USA

[7] Department of Physics and Astronomy, Clemson University, Clemson, SC 29634, USA

[8] Department of Physics and Astronomy, Dickinson College, Carlisle, PA 17013, USA

[9] Universe Cluster, Technische Universität München, Boltzmannstraße 2, 85748 Garching, Germany

[10] Dark Cosmology Centre, Niels Bohr Institute, Univ. of Copenhagen, Juliane Maries Vej 30, 2100 København, Denmark

[11] INAF-IASF Bologna, Area della Ricerca CNR, via Gobetti 101, 40129 Bologna, Italy

[12] Centre for Astrophysics and Cosmology, Science Institute, University of Iceland, Dunhagi 5, 107 Reykjavík, Iceland

[13] American River College, Physics Dpt., 4700 College Oak Drive, Sacramento, CA 95841, USA

[14] Instituto de Astrofísica de Andalucía (IAA-CSIC), Glorieta de la Astronomía s/n, 18.008 Granada, Spain

[15] Institute of Experimental and Applied Physics, Czech Technical University in Prague, Horská 3a/22, 12800 Prague, Czech Republic

[16] INAF – Osservatorio Astrofisico di Arcetri, Largo Fermi 5, 50125 Firenze, Italy

[17] Institute of Astronomy, University of Cambridge, Madingley Road CB3 0HA, Cambridge, UK

[18] Universitá degli Studi di Milano-Bicocca, Piazza della Scienza 2, 20126 Milano, Italy

[19] Scuola Normale Superiore di Pisa – Piazza dei Cavalieri 7, 56126 Pisa, Italy

[20] INAF – Osservatorio Astronomico di Trieste, via G.B. Tiepolo 11, 34143 Trieste, Italy

Appendix A: Additional notes on individual targets: observations by Swift and other facilities

A.1. GRB 050717

GRB 050717 triggered *Swift*/BAT at 10:30:52 UT (Hurkett et al. 2005b). It was a long burst with a duration of $T_{90}(15-350 \text{ keV})$ = (86 ± 2) s (Cummings et al. 2005a) that was also detected by *Konus-WIND* (Golenetskii et al. 2005). *Swift*/XRT began observing 79 s after the trigger and found a bright, fading X-ray source, while simultaneous *Swift* Ultra-Violet/Optical Telescope (UVOT, Roming et al. 2005) observations started 78 s after the trigger and resulted only in upper limits (Hurkett et al. 2005b; Blustin et al. 2005). Unfortunately, XRT was unable to automatically centre on the burst, leading to a delay of 2.5 h in the determination of the X-ray position (error circle radius 6″.0; Kennea et al. 2005; see also Hurkett et al. 2005a). The burst is discussed by Krimm et al. (2006b) in detail; it was very luminous, has one of the highest-ever measured peak energies, and a probable redshift $z > 2.7$. Deep ground-based K-band follow-up observations were performed with the du Pont 100-inch telescope at Las Campanas Observatory with a first run starting 37.7 h after the burst. No fading NIR source was detected (Berger & Lopez-Morales 2005; Berger et al. 2005). Optical observations with the Tenagra 0.35-m telescope at Perth, Australia, did not find a new source down to the limit of the DSS2 red survey (Luckas et al. 2005). In addition, PROMPT-5 at Cerro Tololo Inter-American Observatory in Chile automatically observed the field starting 13 h after the burst. No fading source was found down to $R_C = 21.7$ and $I_C = 21.5$ (MacLeod et al. 2005).

Swift/UVOT obtained an upper limit of $v > 19.0$ for any afterglow at 420 s (mid-time) after the onset of the burst (Blustin et al. 2005), corresponding to $v > 18.3$ after correction for Galactic extinction. Using the observed constraint on the spectral slope $\beta_{OX} < 0.40$ at the time of the UVOT observations, this corresponds to an upper limit of $R_{AB} > 18.2$. In the same way, following Rol et al. (2005), at the time of the optical observation the observed (mean) X-ray flux together with the observed (mean) spectral slope β_X predicts a non-extinguished R_{AB}-band magnitude of between 14.5 ± 1.5 and 18.2 ± 1.5, where the brighter magnitude corresponds to $\nu_c = \nu_{opt}$ and the fainter magnitude to $\nu_c = \nu_X$ (ν_c is the cooling frequency; Sari et al. 1998). According to the criterion of J04, which uses β_{OX}, the burst is dark, while according to the criterion of V09, which uses β_{OX} and β_X, the burst is not dark (Table 2).

A.2. GRB 050922B

Swift/BAT detected the burst at 15:02:00 UT. It was an image trigger lasting for 168 s (Norris et al. 2005). Cummings et al. (2005b) measured $T_{90}(15-150 \text{ keV})$ = (250 ± 20) s. Because of the image trigger history, Norris et al. (2005) speculated that it could be a high-redshift event similar to GRB 050904. *Swift*/XRT started observing 342 s after the trigger, and UVOT one second later (Norris et al. 2005). A decaying X-ray afterglow was detected (Godet et al. 2005) but no optical counterpart (Pasquale et al. 2005). Several ground-based small telescopes responded to the trigger but also failed to find any afterglow candidate, namely ROTSE IIIa (upper limit CR = 17.3 at 3 min; Schaefer et al. 2005), the 14-inch Automated Response Telescope at the University of Osaka, Japan (upper limit CR = 15.1 at 3 min; Torii 2005), the 0.4-m telescope of Ussuriysk Astrophysical Observatory, Russia (upper limit CR = 16.0 at 15 min; Kornienko et al. 2005), and the 30-cm telescope at

University of Miyazaki, Japan (upper limit CR = 16.1 at 21 min; Sonoda et al. 2005).

The INT 2.5-m telescope at Observatorio del Roque de los Muchachos on La Palma obtained an upper limit to the afterglow of $r' > 22.5$ at 49 ks (mid-time) after the onset of the burst (Guziy et al. 2005), corresponding to $r' > 22.4$ after correction for Galactic extinction. There are no X-ray data for the time between about $t = 10$ ks and 100 ks after the burst, but there are for observations from $t \sim 100$ ks to about 1 Ms. The latter data can be used to extrapolate the X-ray flux to $t = 49$ ks. The spectral slope is then $\beta_{OX} < 0.39$, corresponding to an upper limit of about $R_{AB} > 22.3$. Similarly, the observed X-ray flux together with the observed spectral slope β_X at $t = 49$ ks predicts a non-extinguished R_{AB}-band magnitude between 11.1 ± 2.9 and 14.8 ± 3.0. Using β_{OX} and β_X, the burst is dark according to the criterion of J04 as well as V09 (Table 2).

A.3. GRB 060211A

Swift/BAT was triggered by GRB 060211A at 09:39:11 UT (Hurkett et al. 2006). It was a long burst with a duration of T_{90} (15–350 keV) = 126 ± 5 s (Sato et al. 2006a; Krimm et al. 2006a). The spacecraft slewed promptly to the BAT position and *Swift*/XRT found a bright, fading X-ray source, while *Swift*/UVOT started observing 183 s after the trigger but did not detect any afterglow candidate (Hurkett et al. 2006). ROTSE IIIa, located at Siding Spring Observatory, Australia, and the Moscow Union "Optic" MASTER robotic system responded to GRB 060211 immediately. ROTSE's automated response took the first image 147 s after the burst, under twilight conditions, while MASTER started 202 s after the GRB trigger. Only upper limits could be reported (Rujopakarn et al. 2006; Lipunov et al. 2006; see also Urata et al. 2006). In addition, the 2-m Faulkes Telescope North robotically followed-up GRB 060211 starting 5.4 min after the trigger. No fading optical counterpart down to $R \approx 18.5$ was found (Gomboc et al. 2006). Deep upper limits were also reported by Norris et al. (2006), $J > 19.1$ at 17 h after the burst, and Sharapov et al. (2006), $R > 22$ at 5.5 h after the burst.

The 1.5-m telescope of Maidanak Astronomical Observatory obtained for the afterglow an upper limit of $R = 22.0$ at ~20 ks (mid-time) after the onset of the burst (Sharapov et al. 2006), corresponding to $R = 21.6$ after correction for Galactic extinction. This corresponds to an upper limit of $R_{AB} > 21.8$. Among all available upper limits, this observation provides the tightest constraints on the spectral properties of the afterglow from the optical to the X-ray band. According to these data, however, GRB 060211A cannot be classified as a dark burst (Table 2).

A.4. GRB 060805A

The burst triggered *Swift*/BAT on May 8, 2006 at 04:47:49 UT (Ziaeepour et al. 2006). It had a duration of $T_{90}(15-350 \text{ keV})$ = 5.4 ± 0.5 s (Barbier et al. 2006a). *Swift*/XRT began taking data 93 s after the BAT trigger. A ground analysis revealed a faint, uncatalogued X-ray source. *Swift*/UVOT started observing 97 s after the trigger but no afterglow candidate was detected in any band (Ziaeepour et al. 2006; Pandey et al. 2006). Additional ground-based observations could only provide upper limits. The robotic 0.76-m Katzman Automatic Imaging Telescope (KAIT) at Lick Observatory started observing the field 119 s after the BAT trigger but no afterglow was found ($V > 16.8, I > 16.7$; Li 2006). The automated Palomar 60-inch telescope responded

to GRB 060805A and started observing 3 min after the burst trigger. No source down to $R > 19$ was found in the XRT error circle (Cenko 2006). Additional upper limits were obtained by the 1.3-m Skinakas Observatory (University of Crete, Heraklion, Greece) of $R > 21.5$ at 14 h after the burst (Muehlegger et al. 2006) and by the 2-m Liverpool Telescope on La Palma of $r' > 22.9$ and $i' > 22.6$ at 0.725 days and 0.748 days, respectively, after the burst (Rol & Page 2006).

The 2-m Liverpool Telescope observations correspond to $r' > 22.7$, after correction for Galactic extinction. Using $\beta_{OX} < 1.00$, this corresponds to an upper limit of $R_{AB} > 22.7$. Among all available upper limits for this burst, this observation provides the tightest constraint on β_{OX} and β_X (Table 2). However, these constraints do not qualify GRB 060805A as a dark burst, especially because the X-ray afterglow itself was very subluminous.

A.5. GRB 060919

GRB 060919 triggered *Swift*/BAT at 07:48:38 UT (Guidorzi et al. 2006a). It was a long burst with a duration of T_{90} = (15−350 keV) = 9.1 ± 0.2 s (Sato et al. 2006b). *Swift*/XRT began taking data 87 s after the BAT trigger. Ground analysis revealed a faint X-ray source with an revised error circle of $r = 4.''1$ (Guidorzi et al. 2006a,b). *Swift*/UVOT started observing the field 73 s after the burst but did not detect an optical counterpart in any band down to deep flux limits (Breeveld & Guidorzi 2006). The robotic TAROT telescope on La Silla started observing 28 s after the trigger. No optical transient was found down to $R > 15.4$ in the first 60 s of observations. An upper limit of $R > 15.8$ could be set for any transient up to 382 s after the trigger (Klotz et al. 2006). The Faulkes Telescope South started observing about 2.8 h after the event. No optical transient was detected down to a limiting magnitude of $R > 19.5$ (Melandri et al. 2006).

The UVOT upper limit at 918 s corresponds to $v > 20.0$, after correction for Galactic extinction. Using $\beta_{OX} < 0.68$, this corresponds to an upper limit of $R_{AB} > 19.8$. As for to the previous two bursts, this observation provides the tightest constraints achieved to date on the spectral properties of the afterglow. On the basis of these data, GRB 060919 is not a dark burst (Table 2).

A.6. GRB 060923B

Swift/BAT triggered on GRB 060923B at 11:38:06 UT (Stamatikos et al. 2006). It was a single-peaked burst with a duration of $T_{90}(15−350$ keV) = 8.8 ± 0.1 s (Barbier et al. 2006b). *Swift*/XRT began observing the field 114 s after the BAT trigger and found an uncatalogued X-ray source with a positional accuracy of $2.''8$. *Swift*/UVOT started observing 122 s after the burst with the *white* filter but could not detect an afterglow candidate (Stamatikos et al. 2006; Holland & Cucchiara 2006). No further ground-based follow-up observations were reported in the literature.

Swift/UVOT obtained an afterglow upper limit of $v > 18.1$ at 295 s (mid-time) after the burst (Holland & Cucchiara 2006), corresponding to $v > 18.0$ after correction for Galactic extinction. Using $\beta_{OX} < 0.62$, this corresponds to an upper limit of $R_{AB} > 17.9$. Among all available upper limits for this burst this observation provides the tightest constraint on β_{OX} and β_X (Table 2). These constraints do not classify GRB 060923B as a dark event.

A.7. GRB 061102

GRB 061102 triggered *Swift*/BAT at 01:00:31 UT (Holland et al. 2006). It was a long burst with a duration of $T_{90}(15−350$ keV) = 17.6 ± 1 s (Tueller et al. 2006). *Swift*/XRT began observing the field 100 s after the BAT trigger and found an uncatalogued, fading X-ray source (Holland et al. 2006; Starling et al. 2006). *Swift*/UVOT started observing 110 s after the trigger with the *white* filter but no afterglow candidate was seen down to a 3σ upper limit of *white* <18.5 (Holland et al. 2006). Continued observations provided only upper limits in all UVOT bands (Holland 2006). No further ground-based follow-up observations of this event are reported in the literature.

Swift/UVOT obtained an even deeper upper limit of $v > 20.5$ at 1480 s (mid-time) after the onset of the burst (Holland 2006), corresponding to $v > 20.4$ after correction for Galactic extinction. Using the observed $\beta_{OX} < 1.10$, this corresponds to an upper limit of $R_{AB} > 20.1$. Among all available upper limits, this observation provides the tightest constraints on the afterglow SED, which do not classify GRB 061102 as dark (Table 2).

A.8. GRB 070429A

The burst 070429A triggered *Swift*/BAT at 01:35:10 UT (Barthelmy et al. 2007). It was a long burst with $T_{90}(15−350$ keV) = 163 ± 5 s (Cannizzo et al. 2007). *Swift*/XRT started observing 153 s after the trigger and found a fading, uncatalogued X-ray source, while *Swift*/UVOT started observing 211 s after the trigger but did not detect an optical counterpart in any band (Schady & Cannizzo 2007). The ROTSE-IIIc telescope, located at Mt. Gamsberg, Namibia, started observing 97 s after the burst. No afterglow candidate was found down to $CR > 17.3$ (unfiltered images) for images taken within 3 min after the trigger and down to $CR > 18.0$ within 8 min (Rykoff et al. 2007). Additional data were obtained with the 0.6-m BOOTES-IR/T60 robotic telescope (Castro-Tirado et al. 2006), starting 3.25 h after the burst but no afterglow was found (de Ugarte Postigo et al. 2007). Deep K-band observations with the 4.2-m *William Herschel* Telescope on La Palma, beginning 4.1 h after the burst, detected a faint source in the XRT error circle, but no fading behavior was found (de Ugarte Postigo et al. 2007). Within its astrometric errors, this source corresponds to object C detected in our observations (see Table 3).

The Gemini North telescope mounted with the GMOS camera observed the field in i' and z' 44 ks (mid-time) after the burst. No afterglow candidate was found (Price 2007). Unfortunately, no magnitude limits were reported. Therefore, we used a conservative upper limit of $R > 24.0$ based on the original Gemini data available in the Gemini archive[14]. This corresponds to an upper limit of $R_{AB} > 23.8$. Together with the measured X-ray flux at the same time, this leads to $\beta_{OX} < 0.42$ and $\beta_X − \beta_{OX} − 0.5 > 0.14$. According to J04 as well as V09, the burst is dark. The observed X-ray flux predicts a non-extinguished R_{AB}-band magnitude between 17.2 ± 1.5 and 21.0 ± 1.5. Since the *Swift*/XRT light curve shows a constant decay with a constant spectral slope during the time when the optical upper limit was obtained, GRB 070429A is one of three events in our sample that can be securely classified as dark.

---

[14] http://cadcwww.dao.nrc.ca/gsa/

A.9. GRB 070517

This burst triggered *Swift*/BAT at 11:20:58 UT (Vergani et al. 2007a) and T_{90} was 9 ± 1 s (Vergani et al. 2007b). *Swift*/XRT clearly detected an afterglow and could even see evidence of a break in the X-ray light curve. *Swift*/UVOT could not observe because of a 4 mag bright star in the field of view. Ground-based optical follow-up was only reported by Gilmore (2007) (UL = DSS2 Infrared at 2.7 h after the burst) and Fox et al. (2007) using Gemini-South ~16 h after the burst. The latter authors suggested that there were two afterglow candidates in the XRT error circle but no further observations of these sources were reported in the literature. Therefore, we used their faintest detection ($i' > 24.5$) as an upper limit at 57 600 s. Using the corresponding $\beta_{OX} < 0.56$, this translates into an upper limit of $R_{AB} > 24.3$, which does not classify GRB 070517 as a dark burst. However, in our late-time follow-up observations with VLT/FORS1 the brighter object reported by Fox et al. (2007) ($r' = 22.1$) is no longer visible. Thus, we conclude that this was the optical afterglow of GRB 070517.

A.10. GRB 080207

GRB 080207 triggered *Swift*/BAT at 21:30:21 UT (Racusin et al. 2008) and had a duration of $T_{90} = 340 \pm 20$ s (Stamatikos et al. 2008). The XRT started observing the field 124 s after the BAT trigger and detected a bright source in WT mode. After ~5000 s, it continued observing in PC mode, producing a light curve with a constant decay index. *Swift*/UVOT observations did not detect the afterglow both in early observations after 140 s in a *white* finding chart and later deeper observations (>1.5 h, Cucchiara & Racusin 2008). Several limiting magnitudes based on ground-based observations were reported: $R > 14.3$ at 1607 s (0.45 h), and $R > 19.0$ at 5049 s (1.45 h) (TAROT, Calern observatory, Klotz et al. 2008); $J > 16.7$, $H > 15.9$, $K > 13.9$ at 7.8 h, 7.7 h, and 10.1 h after the trigger, respectively (60-cm REM telescope, La Silla, D'Avanzo et al. 2008); $R > 21.8$ at 0.759 h (RTT150 1.5-m telescope, TUBITAK National Observatory, Khamitov et al. 2008); $R > 20.8$ at 13.7 h (Super-LOTIS, Kitt Peak observatory, Updike et al. 2008b); GMOS camera on the Gemini South telescope did not detect the afterglow down to $g'r'i'z' = 24.1, 24.5, 24.2, 25.0$ at 9.8 h (Cucchiara & Fox 2008); $R > 23.5$ at 9.75 h (MOSCA mounted at NOT, La Palma; Marìn et al. 2008); $J > 23.5$, $H > 22.8$, and $K > 21.5$ (VLT/SINFONI, Fugazza et al. 2008); $R > 20.3$ at 1.49 h and $R > 21.0$ at 4.94 h (Zeiss-600 at Mt.Terskol observatory, Andreev et al. 2008). Based on GROND data we did not detect the afterglow in any band down to deep flux limits (Table A.3).

The Zeiss-600 telescope upper limit at 1.69 h corresponds to an upper limit of $R_{AB} > 20.5$. The observed X-ray flux predicts a non-extinguished R_{AB}-band magnitude between 11.3 ± 1.4 and 15.0 ± 1.4. According to the criterion of V09 as well as J04, GRB 080207 is a dark burst (Table 2). It is one of three events in our sample that can be securely classified as dark.

A.11. GRB 080218B

GRB 080218B triggered *Swift*/BAT at 23:57:47 UT and had a duration of $T_{90} = 6.2 \pm 1.2$ s (Schady et al. 2008b). *Swift* slewed immediately to the burst and XRT found a bright, uncatalogued X-ray source that could be localized with an uncertainty of $r = 3\rlap{.}''0$. The *Swift*/UVOT started observing 551 s after the BAT trigger using the *white* filter. No afterglow candidate was

found down to a 3σ limiting magnitude of 20.6 (Schady et al. 2008a). Several limiting magnitudes based on ground-based observations were then reported: $CR > 16$, starting 60 s after the trigger (unfiltered, 0.4-m Watcher telescope, South Africa, French et al. 2008; $I > 21$ and $J > 18.7$ at 3.1 h after the burst (1.3-m SMARTS telescope equipped with ANDICAM at CTIO, Cobb 2008a); $H > 13.7$ at 2 min and $K > 12.6$ at 8 min after the trigger (60-cm REM telescope on La Silla, Covino et al. 2008a); $B > 22.1$, $V > 22.7$, $R > 22.9$, and $I > 22.6$ at about 1 h and $J > 20.6$, $H > 20.1$, and $K_s > 19.4$ at about 3 h after the trigger using VLT/FORS2 and NTT/SOFI (Vreeswijk et al. 2008). Finally, no transient radio source was detected in the XRT error circle two weeks after the burst (Australia Telescope Compact Array, ATCA; Moin et al. 2008). Most importantly, the GROND imager did not detect the afterglow down to deep limits in all seven bands in spite of a rapid response time (Table A.3).

Based on GROND data we obtained an afterglow upper limit of $r' > 24.7$ at 11520 s (mid-time) after the onset of the burst (Rossi et al. 2008b), corresponding to $r' > 24.3$ after correction for Galactic extinction. Using the observed spectral slope $\beta_{OX} < 0.18$, this corresponds to an upper limit of $R_{AB} > 24.3$. The observed X-ray flux predicts a non-extinguished R-band magnitude between 15.1 ± 1.5 and 18.9 ± 1.5. The burst is dark according to the criterion of J04 as well as V09. It is one of three events in our sample that can be securely classified as dark.

A.12. GRB 080602

Swift/BAT triggered the burst at 01:30:28 UT (Beardmore et al. 2008a) and T_{90} was 74 ± 7 s (Beardmore et al. 2008e). The burst was also detected by *Konus-WIND*, observations of this satellite allowing the peak energy to be constrained to be higher than 226 keV (Golenetskii et al. 2008). *Swift*/XRT found a bright, uncatalogued X-ray source resulting in a $5\rlap{.}''8$ error circle. Evidence of substantial X-ray absorption in excess of the Galactic value was found. *Swift*/UVOT started observing 123 s after the trigger but no afterglow candidate was detected. The XRT error circle was finally reduced to only $1\rlap{.}''7$ and $1\rlap{.}''8$, respectively (Beardmore et al. 2008c,d). The only optical follow-up observation was reported by Malesani et al. (2008b) about 3.4 h after the trigger using the NOT telescope on La Palma. No afterglow candidate was found down to $R > 22.3$ (Malesani et al. 2008c).

The *Swift*/UVOT imager obtained an upper limit of $v > 20.3$ at 504 s (mid-time) after the onset of the burst (Beardmore et al. 2008e), corresponding to $v > 20.2$ after correction for Galactic extinction. Using the observed spectral slope of $\beta_{OX} < 0.05$, this corresponds to an upper limit of $R_{AB} > 20.2$. Following Rol et al. (2005), the observed X-ray flux and spectral slope predicts a non-extinguished R_{AB}-band magnitude of between 13.0 ± 0.7 and 16.7 ± 0.7. According to the criterion of J04 as well as V09 the burst is dark (Table 2). However, because the X-ray light curve is rather flat instead of decaying during the time when the optical upper limit was obtained, the burst cannot be securely classified as dark. Unfortunately, no X-ray data was taken contemporaneously with the deep NOT observations.

A.13. GRB 080727A

Swift/BAT triggered on the burst at 05:57:39 UT with a duration (T_{90}) of 4.9 ± 1.0 s. About 109 s later, *Swift*/XRT began observing the field (Immler et al. 2008), unveiling a light curve with constant decay and evolving spectral index (see the XRT repository, Evans et al. 2007, 2009). The UVOT imager started observing

at 113 s, no afterglow being found (Landsman & Immler 2008). In addition, UKIRT on Mauna Kea did not detect the afterglow down to $K > 19.8$ at 0.63 h after the trigger (Levan & Wiersema 2008). FORS1 on ESO/Paranal observed the field at 17.5 h and did not detect the afterglow down to the very deep upper limit of $R > 26$ (Malesani et al. 2008a).

Using the observed spectral slope $\beta_{OX} < 0.85$, the UKIRT upper limit corresponds to an upper limit of $R_{AB} > 22.8$. Following Rol et al. (2005), the observed X-ray flux and spectral slope at the time when the optical upper limit was obtained predicts a non-extinguished R_{AB}-band magnitude of between 17.9 ± 2.2 and 21.6 ± 2.2. According to the criterion of V09, the burst lies at the boundary region between dark and non-dark events ($\Delta_{min} = -0.05$; Table 2). Unfortunately, no X-ray data was taken contemporaneously with the deep VLT observations.

A.14. GRB 080915A

GRB 080915A triggered *Swift*/BAT at 00:02:49 UT (Oates et al. 2008a). It was a long burst with a duration of $T_{90} = (15-350 \text{ keV}) = 14 \pm 5$ s (Ukwatta et al. 2008). Unfortunately, owing to an observing constraint, *Swift* could not slew to the burst during the first hour after the event, therefore XRT and UVOT could start observing only 3.9 ks after the trigger. Starting at this time, *Swift*/UVOT did not detect the optical afterglow (Oates et al. 2008b). The ROTSE-IIIc telescope located on Mt. Gamsberg, Namibia, responded to GRB 080915A automatically and took unfiltered images starting 52 s after the GRB trigger (cloudy conditions, full Moon). No afterglow candidate was found in the BAT error circle down to about $CR > 14$ (Rujopakarn et al. 2008). The robotic 60-cm REM telescope on La Silla started observing 2 min after the trigger. No afterglow candidates fainter than the 2MASS limits were seen in J, H, K (Covino et al. 2008b). Beginning 4.9 ks after the trigger, *Swift*/XRT and *Swift*/UVOT started observing. XRT found a faint, fading X-ray source with an error circle of $r = 6''.5$ (Evans & Oates 2008). Only upper limits could be reported for the UVOT bands (Breeveld & Oates 2008). Deep ground-based observations with ANDICAM on the SMARTS 1.3-m telescope at CTIO provided only upper limits of $I > 21.9$ and $J > 20.1$ (mid-time of 1.9 h after the burst; Cobb 2008b).

Deep prompt follow-up observations of the field were performed with GROND (Rossi et al. 2008c). They started 4.9 min after the trigger and lasted for 130 min. No evidence of a variable source was found when splitting these observations into two data sets (Table A.3). Second-epoch observations were performed with GROND the following night. Again, no afterglow candidate was found. Using the GROND upper limit of $r'_{AB} > 22.2$ at 6840 s (mid-time; Rossi et al. 2008c), and $\beta_{OX} < 0.62$ (Table 2), this corresponds to an upper limit of $R_{AB} > 22.0$. Following Rol et al. (2005), we can use the observed X-ray flux as well as the X-ray slope to predict the non-extinguished R_{AB}-band magnitude. However, in this case owing to the small number statistics we can only give an upper limit of $R_{AB} < 21$. According to the criterion of V09, the burst is dark (Table 2), but the X-ray light curve is faint and very uncertain. Therefore, this burst cannot be securely classified as dark.

A.15. GRB 081012

Swift/BAT triggered on the burst at 13:10:23 UT. T_{90} (15–350 keV) was 29 ± 4 s. The burst was also seen by Fermi/GBM, the peak energy was 320 ± 80 keV (Bissaldi 2008). The XRT began observing the field 49 min after the BAT trigger, an X-ray

afterglow was found (Kennea & Stroh 2008), the error circle is just $1''.8$ in size (Evans et al. 2008). The UVOT started observing 3 min after the XRT; no afterglow candidate was detected (Kuin & Stroh 2008). Deep ground-based follow-up observations were performed using ROTSE IIIa (starting 39 s after the burst), the 2.5-m NOT telescope (de Ugarte Postigo & Malesani 2008).

The GROND imager obtained an upper limit on any optical afterglow of $r'_{AB} > 23.6$ at ~70 ks (mid-time) after the onset of the burst (Filgas et al. 2008; Table A.3), corresponding to $r' = 23.5$ after correction for Galactic extinction. Using the observed spectral slope of $\beta_{OX} < 0.83$, this corresponds to an upper limit of $R_{AB} > 23.4$. Among all available optical upper limits, this observation provides the tightest constraint on the SED of the afterglow (Table 2). On the basis of these data, this burst is not dark.

A.16. GRB 081105

This burst triggered *Konus-WIND*, *Swift*, *AGILE*, *Suzaku*, and *INTEGRAL* at 13:26:12 UT. It was localized only via IPN. The burst had a single peak, about 10 s long (Cummings et al. 2008). *Swift*/XRT and UVOT started observing the field about 16 h later. An X-ray afterglow candidate was detected with an original uncertainty of $4''.8$ (Beardmore & Cummings 2008) and later confirmed (Beardmore et al. 2008b). Observations with UVOT could only provide upper limits (Curran et al. 2008).

The GROND imager obtained an afterglow upper limit of $r' > 23.0$ at ~46 ks (mid-time) after the burst (Clemens et al. 2008; Table A.3), corresponding to $r' > 22.9$ after correction for Galactic extinction. Using $\beta_{OX} < 0.61$, this corresponds to an upper limit of $R_{AB} > 22.8$. This observation provides the tightest constraints on the SED. On the basis of these data, the burst is not dark (Table 2).

A.17. GRB 081204

The burst was detected by the *INTEGRAL* satellite at 16:44:55 UT. It lasted for about $T_{90} = 20$ s (Götz et al. 2008). *Swift* reacted to the Integral alert, and started observing the field about 2.7 h after the burst, and found an uncatalogued X-ray source (Mangano et al. 2008a,b). *Swift*/UVOT started observing 3 h after the trigger in the *white* filter but no source was detected. Berger & Rest (2008) suggested an $r = 23.5 \pm 0.3$ afterglow candidate based on observations with the Magellan/Clay telescope about 9 h after the trigger.

The field was also observed with GROND, which also detected the afterglow candidate observed by Berger & Rest (2008), together with another object, without finding evidence of fading in either source (Updike et al. 2008a). Both objects are discussed in this paper as host candidates (see Sect. 3.3). Stacking the highest quality GROND data, we obtained the revised upper limits reported in Table A.3, centered at a mid-time of 9.6 h. The GROND upper limit of $r' > 24.1$ corresponds to $r' > 24.0$ after correction for Galactic extinction. Using the observed $\beta_{OX} < 0.55$, this corresponds to an upper limit of $R_{AB} > 23.9$. Following Rol et al. (2005), we can use the observed X-ray flux as well as the X-ray slope to predict the non-extinguished R_{AB}-band magnitude. However, in this case owing to the small number statistics we can only give an upper limit of $R_{AB} < 23$ in the worse case of a break between optical and X-ray bands. The burst is dark according to V09 (Table 2), but owing to the faint XRT light curve and the poorly determined high X-ray spectral slope ($\beta_X = 1.93^{+1.56}_{-0.77}$) this burst cannot be securely classified as dark.

Table A.1. Redshifts estimated via the Amati relation.

#	GRB	Data	Model	E_{peak}(keV)	Redshift
2	050922B	BAT	Band	~ 20	$0.1 < z < 3$
6	060923B	BAT	CPL	25 ± 7	$z > 0.4$
10	080207	BAT	CPL	108 ± 72	$z > 0.9$
11	080218B	BAT	CPL	24 ± 15	$z > 0.3$
12	080602	KW	CPL	>226	$z > 1$

Notes. BAT stands for *Swift*/BAT, KW for *Konus-Wind* and CPL for cut-off power-law.

Table A.2. Redshift estimates of the galaxies found in the XRT error circles for different model assumptions about their photometric properties.

#	GRB	Object	(4)	(5)	(6)	(7)	(8)	(9)
1	050717	A	0.5	0.4	1.2	0.9	3.2	1.8
		B	0.7	0.6	1.7	1.2	–	2.4
3	060211	A	0.7	0.6	1.7	1.2	–	2.4
		B	0.4	0.3	0.9	0.7	2.3	1.4
4	060805A	A	0.9	0.7	2.3	1.4	–	3.0
		B	0.5	0.4	1.1	0.8	3.1	1.8
5	060919	A	1.5	1.0	4.2	2.1	–	4.5
6	060923B	A	0.4	0.3	0.9	0.7	2.4	1.5
		C	0.7	0.6	1.7	1.2	–	2.4
		D	1.2	0.9	3.3	1.8	1.5	3.9
7	061102	A	0.6	0.5	1.4	1.0	4.1	2.1
		B	0.5	0.5	1.3	1.0	3.8	2.0
8	070429A	A	0.9	0.7	2.2	1.4	–	2.9
		B	0.6	0.5	1.5	1.0	4.2	2.1
		C	0.6	0.5	1.6	1.1	4.7	2.3
9	070517	A	1.0	0.8	2.7	1.6	–	3.4
10	080207	A	0.9	0.7	2.4	1.5	–	3.1
		B	1.7	1.1	–	2.4	–	–
11	080218B	A	1.5	1.1	4.4	2.2	–	4.7
		B	0.7	0.6	1.8	1.2	–	2.5
12	080602	A	0.4	0.3	0.8	0.7	2.2	1.4
		B	0.6	0.5	1.4	1.0	3.9	2.0
14	080915A	B	0.2	0.2	0.4	0.4	1.0	0.7
		C	0.8	0.6	1.9	1.3	–	2.6
		D	0.7	0.6	1.8	1.2	–	2.5
		E	1.0	0.8	2.8	1.6	–	3.5
15	081012	A	0.9	0.7	2.4	1.5	–	3.1
16	081105	A	0.5	0.4	1.2	0.9	3.3	1.8
		B	0.6	0.5	1.6	1.1	4.7	2.3
17	081204	A	0.4	0.3	0.9	0.7	2.5	1.5
		B	0.4	0.4	1.1	0.8	2.9	1.7
		C	0.4	0.3	0.9	0.7	2.4	1.5
		D	0.6	0.5	1.5	1.0	4.3	2.2
		E	0.6	0.5	1.6	1.1	4.7	2.3
		F	1.1	0.8	3.1	1.7	–	3.7

Notes. Columns (4) to (9) give the redshift of the galaxy for different assumptions about its spectral slope β and absolute magnitude M_R: = (0.0, −18), (1.0, −18), (0.0, −20), (1.0, −20), (0.0, −22), (1.0, −22). For greater detail, see Sect. 4.6. GRB 050922B and GRB 080727A are not included here since they have no host galaxy candidates.

Table A.3. Summary of the early-time upper limits based on observations with GROND.

#	GRB	t [h]	Filter	UL
10	080207	9.75	g'	24.0
		9.75	r'	23.6
		9.75	i'	23.1
		9.75	z'	22.3
		9.75	J	21.0
		9.75	H	19.7
		9.75	K_{s}	19.0
11	080218B	0.75	g'	21.4
		0.75	r'	21.5
		0.75	i'	20.6
		0.75	z'	20.6
		0.75	J	20.8
		0.75	H	18.5
		0.75	K_{s}	17.8
		3.2	g'	24.6
		3.2	r'	24.7
		3.2	i'	23.9
		3.2	z'	24.7
		3.2	J	22.0
		3.2	H	20.8
		3.2	K_{s}	20.0
14	080915A	0.15	g'	22.0
		0.15	r'	22.2
		0.15	i'	21.8
		0.15	z'	21.7
		0.15	J	20.1
		0.15	H	18.9
		0.15	K_{s}	17.6
		0.92	g'	23.0
		0.92	r'	23.5
		0.92	i'	23.0
		0.92	z'	23.1
		0.92	J	21.2
		0.92	H	20.0
		0.92	K_{s}	18.6
15	081012	19.35	g'	23.2
		19.35	r'	23.5
		19.35	i'	22.8
		19.35	z'	22.8
		19.35	J	21.5
		19.35	H	20.4
		19.35	K_{s}	19.4
16	081105	12.84	g'	24.0
		12.84	r'	23.0
		12.84	i'	22.1
		12.84	z'	21.8
		12.84	J	20.7
		12.84	H	19.6
		12.84	K_{s}	18.2
17	081204	9.60	g'	24.2
		9.60	r'	24.1
		9.60	i'	23.2
		9.60	z'	22.4
		9.60	J	20.7
		9.60	H	19.4
		9.60	K_{s}	18.3

Notes. For early-time observations by other groups see, e.g., the web page of Greiner at www.mpe.mpg.de/~jcg/grbgen.html or GRBlog at http://grblog.org/grblog.php. In all cases, the data given here supersede the values given in the corresponding GRB circulars: GCN 7279, GRB 080207 (Küpcü Yoldaş et al. 2008); GCN 7319, GRB 080218B (Rossi et al. 2008b); GCN 8268, GRB 080915A (Rossi et al. 2008c); GCN 8373, GRB 081012 (Filgas et al. 2008); GCN 8492, GRB 081105 (Clemens et al. 2008); GCN 8627, GRB 081204 (Updike et al. 2008a).

Table A.4. Log of the late-time optical/NIR observations to search for a GRB host candidate.

#	GRB	Instrument	Filter	Date obs	Calib	*FWHM*	Exp. (s)
1	050717	GROND	$g'r'i'z'$	2007/07/24-26	SA114-750	1''0	8880
		GROND	JHK_s	2007/07/24-26	2MASS	1''4	7200
2	050922B	FORS2	R_C	2009/08/15	ESO ZP	0''7	2930
		ISAAC	K_s	2009/07/06	2MASS	0''7	1920
		NEWFIRM	K_s	2008/11/08	2MASS	1''2	1800
3	060211A	GROND	$g'r'i'z'$	2007/10/20-22	SA95-190	1''0	10 360
		GROND	JHK_s	2007/10/20-22	2MASS	1''6	8400
		NEWFIRM	J	2009/01/17	2MASS	1''1	10 200
		NEWFIRM	K_s	2009/01/17	2MASS	1''2	3600
4	060805A	GROND	$g'r'i'z'$	2008/05/05-07	SDSS	0''9	4440
		GROND	JHK_s	2008/05/05-07	2MASS	1''6	3600
5	060919	FORS1	R_C	2008/04/10	SA110-362	0''8	2930
		ISAAC	K_s	2008/05/18	2MASS	0''6	1920
6	060923B	FORS1	R_C	2008/04/05	NGC2437	0''8	2930
		ISAAC	K_s	2008/04/15	2MASS	0''5	1920
7	061102	FORS1	R_C	2008/04/06	NGC2437	0''7	2930
		ISAAC	K_s	2008/04/18	2MASS	0''7	1920
8	070429A	FORS1	R_C	2008/04/08	SA110-362	1''0	2930
		ISAAC	K_s	2008/05/18	2MASS	0''6	2400
9	070517	FORS1	R_C	2008/04/10	SA110-362	0''6	2930
		ISAAC	K_s	2008/08/05	2MASS	0''5	1920
10	080207	VIMOS	R_C	2010/02/10	PG1047+3	0''8	2930
		ISAAC	K_s	2010/02/07	2MASS	0''6	1920
11	080218B	FORS2	R_C	2009/05/26	PG1047	0''5	2930
		ISAAC	K	2009/03/20	2MASS	0''5	1920
12	080602	GROND	$g'r'i'z'$	2009/11/24	SDSS	1''1	4440
		GROND	JHK_s	2009/11/24	2MASS	1''3	3600
		FORS2	R_C	2009/06/05	NGC7006	0''8	2930
		ISAAC	K_s	2009/07/06	2MASS	0''7	1920
13	080727A	FORS1	R_C	2008/07/27	E5-Stetson	0''8	2930
		ISAAC	K_s	2010/02/10	2MASS	0''6	1920
14	080915A	FORS1	R_C	2008/09/27	E7	1''4	968
		HAWK-I	K_s	2008/09/16	2MASS	0''6	840
15	081012	VIMOS	R_C	2009/10/21	SA98	0''8	2400
		ISAAC	K_s	2009/10/08	2MASS	0''4	1920
16	081105	VIMOS	R_C	2009/10/21	SA98	1''0	2400
		ISAAC	K_s	2009/09/14	2MASS	0''4	1920
17	081204	VIMOS	R_C	2009/10/21	SA98	1''0	2400
		ISAAC	K_s	2009/09/14	2MASS	0''5	1920
		SOFI	J	2010/11/01	2MASS	0''5	3600

Notes. *Notes for individual targets:* GRB 070517: a candidate optical afterglow was found by Fox et al. (2007), which we identify as the GRB afterglow based on our data. *Standard star fields:* the fields PG1047+3, E5, E7, NGC 2437, and NGC 7006 are from the internet pages of Stetson http://www3.cadc-ccda.hia-iha.nrc-cnrc.gc.ca/community/STETSON/. Landolt equatorial standards stars (SA) for the R_C band were obtained from the internet page of the Canada-France-Hawaii Telescope http://www.cfht.hawaii.edu/ObsInfo/Standards/Landolt/. SA standard star fields for GROND optical calibrations are downloaded from the SDSS archive server at http://www.sdss.org/. ZP stands for photometric zero-point calibration. *Filters:* observations with FORS2 were performed using the $R_{special+76}$ filter. Both, FORS1 and VIMOS used the $R_{Bessel+36}$ filter. The FWHM column refers to the FWHM of the average stellar PSF.